Science of the Total Environment 605–606 (2017) 124–138

Contents lists available at ScienceDirect

Science of the Total Environment

journal homepage: www.elsevier.com/locate/scitotenv

First results from light scattering enhancement factor over central Indian Himalayas during GVAX campaign

U.C. Dumka [a,*], D.G. Kaskaoutis [b], Ram Sagar [a,c], Jianmin Chen [d,e], Narendra Singh [a], Suresh Tiwari [f]

[a] Aryabhatta Research Institute of observational Sciences, Nainital 263 001, India
[b] Atmospheric Research Team, Institute for Environmental Research and Sustainable Development, National Observatory of Athens, 118 10 Athens, Greece
[c] NASI-Senior Scientist Platinum Jubilee Fellow, Indian Institute of Astrophysics, Bangalore 560 034, India
[d] Shanghai Key Laboratory of Atmospheric Particle Pollution and Prevention, Department of Environmental Science and Engineering, Institute of Atmospheric Sciences, Fudan University, Shanghai 200 433, China
[e] Collaborative Innovation Center of Climate Change, School of Atmospheric Sciences, Nanjing University, Nanjing 210 023, China
[f] Indian Institute of Tropical Meteorology, Pune, New Delhi Branch, New Delhi 110 060, India

HIGHLIGHTS

- Study on aerosol hygroscopicity for the first time over the central Himalayas
- Slightly larger light scattering enhancement factor f(RH) values for the fine particles
- Increase in aerosol hygroscopicity under more turbid atmospheres

GRAPHICAL ABSTRACT

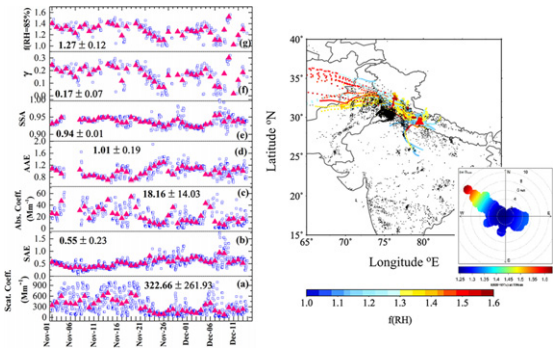

ARTICLE INFO

Article history:
Received 5 April 2017
Accepted 17 June 2017
Available online 27 June 2017

Editor: D. Barcelo

Keywords:
Aerosol hygroscopicity
Scattering enhancement
f(RH = 85%)
Relative humidity
CCN
GVAX
Himalaya

ABSTRACT

The present work examines the influence of relative humidity (RH), physical and optical aerosol properties on the light-scattering enhancement factor [f(RH = 85%)] over central Indian Himalayas during the Ganges Valley Aerosol Experiment (GVAX). The aerosol hygroscopic properties were measured by means of DoE/ARM (US Department of Energy, Atmospheric Radiation Measurement) mobile facility focusing on periods with the regular instrumental operation (November–December 2011). The measured optical properties include aerosol light-scattering (σ_{sp}) and absorption (σ_{ap}) coefficients and the intensive parameters i.e., single scattering albedo (SSA), scattering Ångström exponent (SAE), absorption Ångström exponent (AAE) and light scattering enhancement factor ($f(RH) = \sigma_{sp}(RH, \lambda)/\sigma_{sp}(RH_{dry}, \lambda)$). The measurements were separated for sub-micron (<1 μm, $D_{1\ \mu m}$) and particles with diameter < 10 μm ($D_{10\ \mu m}$) in order to examine the influence of particle size on f(RH) and enhancement rate (γ). The particle size affects the aerosol hygroscopicity since mean f(RH = 85%) of 1.27 ± 0.12 and 1.32 ± 0.14 are found for $D_{10\ \mu m}$ and $D_{1\ \mu m}$, respectively. These f(RH) values are relatively low suggesting the enhanced presence of soot and carbonaceous particles from biomass burning activities, which is verified via backward air-mass trajectories. Similarly, the light-scattering enhancement rates are ~0.20 and 0.17 for the $D_{1\ \mu m}$ and $D_{10\ \mu m}$ particles, respectively. However, a general tendency for increasing f(RH) and γ is shown for higher σ_{sp} and σ_{ap} values indicating the presence of rather aged smoke plumes, coated with industrial aerosols over northern India, with mean SSA, SAE and AAE values of 0.92, 1.00 and 1.15 respectively. On the other hand, a moderate-to-small dependence of f(RH) and γ on SAE, AAE, and SSA was observed

* Corresponding author at: ARIES, Manora Peak, Nainital 263 001, Uttarakhand, India.
E-mail address: dumka@aries.res.in (U.C. Dumka).

http://dx.doi.org/10.1016/j.scitotenv.2017.06.138

for both particle sizes. Furthermore, f(RH) exhibits an increasing tendency with the number of cloud condensation nuclei (N_{CCN}) indicating larger particle hygroscopicity but without significant dependence on the activation ratio.

1. Introduction

Atmospheric research in the south and southeast Asia has gained importance during the last decades due to the rapid urbanization, industrialization, increasing emission rates and contribution to Asian pollution outflow and atmospheric brown clouds (Lelieveld et al., 2001; Lawrence and Lelieveld, 2010; Lu et al., 2011 and references therein). More particularly, the Indo-Gangetic Plain (IGP) region is considered as one of the aerosol hotspot areas over the globe (Dey and Di Girolamo, 2010; Kaskaoutis et al., 2014a), where significant mixing of aerosols of various origin and composition (natural dust, black carbon, organic matter, sulfates, nitrates, ammonium, etc) exists, resulting in hazy atmospheres under certain conditions (Ram et al., 2010a, 2010b). This high aerosol loading, composed of a significant fraction of absorbing aerosol, leads to perturbations on monsoon onset, duration and intensity particularly over the northern India and Himalayas (Gautam et al., 2009) and to the continuation of the solar dimming effect (Kambezidis et al., 2012). Despite numerous studies, large uncertainties still exist in the aerosol-climate implications over this region due to large heterogeneity in aerosol types, complexity in their microphysical, hygroscopic properties and aerosol-cloud-precipitation interactions.

The knowledge of the role of relative humidity (RH) on aerosol hygroscopicity, optical properties and light-scattering enhancement is of great importance for understanding the aerosol effects (direct and indirect) on regional climate (Wang and Martin, 2007; Fierz-Schmidhauser et al., 2010a; Zieger et al., 2011, 2012; Esteve et al., 2012; Shinozuka et al., 2013), as well as for issues related to effects of aerosol water uptake on public health (Youn et al., 2016). Aerosol light-scattering enhancement due to water uptake results in more efficient scattering in the atmosphere and reduction of solar radiation reaching the ground (Titos et al., 2014a; Zieger et al., 2014), while the aerosol hygroscopicity determines their ability to act as cloud condensation nuclei, thus modifying cloud albedo, lifetime and precipitation onset (Lohmann and Feichter, 2005; Rosenfeld et al., 2008). Aerosols uptake water as RH increases, thereby growing in diameter and enhance their scattering ability and single scattering albedo (SSA). The impact of RH on aerosol scattering coefficient (σ_{sp}) is represented by the light scattering enhancement factor or humidification factor f(RH), which is defined as the ratio between the σ_{sp} at high RH (~85%) and reference RH (~40%), thus quantifying the change in σ_{sp} due to the water uptake. In this respect, long-term measurements of aerosol optical and physical properties from the World Meteorological Organization's/Global Atmosphere Watch program (WMO/GAW, 2003) recommend that aerosol measurements should be performed at dry conditions (RH < 40%) and for inclusion of aerosol measurements in climate models, the influence of RH must be taken into account. However, most of the satellite algorithms omit hygroscopic properties of ambient aerosols in their retrievals, while the incorporation of in-situ knowledge of RH in aerosol retrieval algorithms is encouraged, especially over urban areas (Wang and Martin, 2007). However, detailed information of aerosol hygroscopicity is insufficiently used in the general circulation models that call for more comprehensive description and parameterization of this parameter.

During the last decade, several studies have been carried out to assess the impact of RH on σ_{sp} in various worldwide locations and for different aerosol types, such as urban (e.g., Sheridan et al., 2001; Yan et al., 2009; Zieger et al., 2011; Tijjani and Uba, 2013; Titos et al., 2014b), free tropospheric (Fierz-Schmidhauser et al., 2010b), continental (Koloutsou-Vakakis et al., 2001; Pan et al., 2009; Zieger et al., 2012; Tijjani et al., 2014), marine (Fierz-Schmidhauser et al., 2010c), mineral dust and pollution (Carrico et al., 2003; Kim et al., 2006; Fierz-Schmidhauser et al., 2010b; Zieger et al., 2012) and biomass burning (Kotchenruther and Hobbs, 1998; Kim et al., 2006; Carrico et al., 2008). There are several in situ measurements dealing with f(RH), but very few focused on aerosol scattering enhancement of fine-mode aerosols, although some exceptions can be found in the literature (Koloutsou-Vakakis et al., 2001; Sheridan et al., 2001; Carrico et al., 2003; Titos et al., 2014a), but are very sparse over the Indian subcontinent (Titos et al., 2016).

In this work, aerosol optical, physical and hygroscopic properties for two size ranges ($D_{1\ \mu m}$; diameter < 1 μm and $D_{10\ \mu m}$; diameter < 10 μm) were examined at an elevated (1958 m) Himalayan site (Nainital) in the framework of Ganges Valley Aerosol Experiment (GVAX), which took place from June 2011 to March 2012. The scientific contribution of the current work against previous publications of the GVAX campaign (Dumka and Kaskaoutis, 2014; Manoharan et al., 2014; Dumka et al., 2015a, 2015b; Gogoi et al., 2015) is the first-time examination of the hygroscopic light-scattering enhancement or humidification factor f(RH) in the central Gangetic-Himalayan (CGH) region. The datasets are analyzed on hourly and daily basis during the period 1 November–13 December 2011, thus examining the influence of the changes in aerosol optical properties and meteorological conditions on particle's hygroscopicity. The main objectives of the present work are i) to estimate the values of f(RH) and γ and examine their temporal variation focusing on November–December period, ii) to explore the different atmospheric conditions and air-mass trajectories that led to changes in the aerosol hygroscopicity and, iii) to examine the role of RH, particle size, scattering and absorption coefficients, SSA, N_{CCN} on aerosol light-scattering enhancement.

2. Theoretical background

Under humid atmospheres, aerosol particles can uptake water depending on their size and chemical composition, thus increasing in size from their dry equivalents; this procedure leads to enhanced scattering and change in the geometry of the scattered light increasing the forward part (Titos et al., 2016). Certain aerosol types like desert dust and soot (Black Carbon, BC) are considered as insoluble particles that do not uptake water and do not significantly increase in size with increasing RH (e.g., Zieger et al., 2013; Titos et al., 2014b, 2016). A recent paper (Shingler et al., 2016a) showed that under certain atmospheric conditions dominated by hydrophobic carbonaceous particles, f(RH) values < 1 might also been observed indicating particle shrinkage. In contrast, some organics (i.e., water soluble Organic Carbon, WSOC) and inorganic salts are hygroscopic particles and can increase in diameter as the RH increases. Further, a specific category is composed by the so-called "deliquescent aerosols" like sodium chloride (NaCl) or ammonium sulfate $(NH_4)_2SO_4$, which are hygroscopic particles but exhibit a sudden phase transition from solid to liquid at a defined RH (e.g., Zieger et al., 2013; Titos et al., 2016). The dependence of aerosol light scattering on RH is an essential parameter for accurate estimation of the direct radiative forcing induced by aerosol particles. On the other hand, f(RH) represents the overall aerosol light-scattering enhancement factor for the aerosol population and is determined by the particle number size distribution (PNSD), chemical composition, density and refractive index. Moreover, changes in particle's morphology may also affect the aerosol optical and hygroscopic properties leading to significant

impact on f(RH) (Chen et al., 2014). Overall, the f(RH) is mostly sensitive to variations in hygroscopic growth factor and refractive index (Fierz-Schmidhauser et al., 2010c). The effect of RH on light scattering can be determined by means of two Nephelometer systems operated in parallel or in series and separated by a humidifier system (Liu et al., 2009; Jefferson, 2011; Sheridan et al., 2001; Chen et al., 2014; Titos et al., 2014a, 2014b); one Nephelometer measures at a reference RH (≤40%), while the other measures at a higher RH (~80–85%). The combination of these two measurements allows the determination of f(RH) via Eq. (1):

$$f(RH,\lambda) = \frac{\sigma_{sp}(RH,\lambda)}{\sigma_{sp}(RH_{dry},\lambda)} \quad (1)$$

where $\sigma_{sp}(RH, \lambda)$ is the aerosol light-scattering coefficient at a certain wavelength λ and RH and $\sigma_{sp}(RH_{dry}, \lambda)$ is the corresponding scattering coefficient measured at dry conditions (RH ~ ≤40%). The humidification factor can be parameterized by means of an empirical power-law fit that is commonly used in the literature (e.g., Hänel and Zankl, 1979; Clarke et al., 2002; Carrico et al., 2003; Zieger et al., 2011; Titos et al., 2014a, 2014b) to describe RH dependence on f(RH) (Eq. (2)), although several other formulas have been also proposed (Titos et al., 2016):

$$f(RH,\lambda) = a\left\{1-\frac{RH\%}{100}\right\}^{-\gamma} \quad (2)$$

where "γ" and "a" are two independent fitting parameters. The parameter "a" accounts for the intercept at RH = 0% and "γ" represents the magnitude of the light-scattering enhancement rate. Although Carrico et al. (2003) suggested several other fitting techniques applied to different RH ranges, the scattering enhancement procedure due to aerosol hygroscopic growth is described satisfactorily by Eq. (2); however, it is unable to reproduce the aerosol deliquescence process for the whole RH range (Kotchenruther et al., 1999; Titos et al., 2016).

3. Measurements and instrumentation

In-situ measurements of aerosol optical and physical properties were carried out at Manora Peak (29.4°N; 79.5°E; ~1958 m above mean sea level), Nainital using the U. S. Department of Energy Atmospheric Radiation Measurements (http://www.archive.arm.gov) Program Mobile Facility during the GVAX campaign (https://www.arm.gov/sites/amf/pgh). GVAX aimed at investigating the impact of aerosol on regional climate, the contribution of Ganges Valley to aerosol plumes over the Himalayas and the physical processes of aerosol-cloud interactions (Dumka et al., 2015a; Gogoi et al., 2015; Moorthy et al., 2016). Nainital is an ideal site for studying the impact of local and transported aerosol plumes and the role of boundary-layer dynamics in determining the aerosol properties and radiation budget, since during specific time periods (i.e., wintertime, early morning and late evening) it is located above the polluted IGP boundary layer (Dumka et al., 2015a, 2015b). The Aerosol Observing System (AOS; http://www.arm.gov/publications/tech_reports/handbooks/aos_handbook.pdf; Anderson and Ogren, 1998; Jefferson, 2011), was used in the campaign, which provided measurements of several optical and physical aerosol properties, like light scattering (σ_{sp}) and absorption (σ_{ap}) coefficients for two particle-size groups ($D_{1\ \mu m}$ and $D_{10\ \mu m}$), from which several other parameters can be obtained i.e., SSA, scattering Ångström exponent (SAE), absorption Ångström exponent (AAE), sub-micron fraction, etc. (Dumka and Kaskaoutis, 2014; Dumka et al., 2015a). The aerosol samples passed through an inertial impactor with 5-min switching frequency and cut-off particle diameters at either 1 μm ($D_{1\ \mu m}$) or 10 μm ($D_{10\ \mu m}$), before the light scattering and absorption measurements were performed. Further details about this separation can be found in previous studies (Dumka and Kaskaoutis, 2014; Dumka et al., 2015a, 2015b).

The σ_{sp} and backscattering coefficient (σ_{bsp}) were measured via integrating Nephelometer (TSI; Model 3563) at three wavelengths (450, 550 and 700 nm) (Anderson et al., 1996). The σ_{ap} values were measured via three wavelengths (467, 530 and 660 nm) particle soot absorption photometer (PSAP). Furthermore, number concentrations of the condensation nuclei (N_{CN}) in diameter range 0.01–3.0 μm and cloud condensation nuclei (N_{CCN}) have been also measured using a compact and rugged butanol-based Condensation Particle Counter (CPC, model 3010; TSI made) and CCN counter (Droplet Measurement Technology; DMT; Robert and Nenes, 2005), respectively. CPC has a high signal-to-noise ratio that attains accurate detection of small particles and its upper concentration limit is 10,000 particles per cm^3. The CCN counter measures activated particle concentrations being converted to cloud droplets by condensation of water at a given saturation (S); four S levels have been used and more details are given elsewhere (Dumka et al., 2015b). The N_{CCN} measurements were considered at 5-min intervals (1-min measurements averaged into 5 min) for each S level, while N_{CN} were measured continuously (1-min time interval, also averaged for 5 min) by the CPC. In this work, the N_{CCN}, N_{CN} and the activation ratio ($AR = N_{CCN}/N_{CN}$) are considered at 0.31–0.33% S and are used for comparison with the f(RH = 85%) retrievals.

For examining the aerosol hygroscopicity, two integrating Nephelometers were deployed in series and connected with a humidifier system between them. However, a heating system along with humidity sensor was used to produce dry air before the particle reached the reference Nephelometer. Subsequently, the output air of the reference Nephelometer is passed through the humidifier under the temperature and RH controlled environment and given as an input to the second Nephelometer (Jefferson, 2011; Dumka and Kaskaoutis, 2014). The first Nephelometer serves as the "reference" measuring σ_{sp} at low RH (RH < ~40% as recommended by WMO/GAW, 2003), while the second measures changes in σ_{sp} with RH, as it scans RH from low (≤40%) to high (85%) values and then back to low RH on an hourly basis (Jefferson, 2011). The estimation of f(RH) is affected by multiple error sources such as (i) the Nephelometer uncertainty in measuring the particle scattering coefficient (~10%, Anderson et al., 1996), (ii) errors in the reference-Nephelometer RH values, (iii) uncertainties in RH in the humidified Nephelometer (1.5–2 of RH, Fierz-Schmidhauser et al., 2010c), (iv) possible particle loss in the humidification system and, (v) errors in the residence time that aerosols spend in the humidification system in order to reach the equilibrium RH (Titos et al., 2016). Furthermore, evaporation of semi-volatile components in the sampling lines and in the instrument itself may be an additional source of uncertainty in f(RH) and γ estimations (Shingler et al., 2016a). Some authors have reported higher losses in the humidification system for $D_{10\ \mu m}$ rather than $D_{1\ \mu m}$ (e.g., Carrico et al., 2003; Titos et al., 2014a), while previous studies (Zieger et al., 2010, 2013; Titos et al., 2016) also revealed that the uncertainty in f(RH) increases with the increasing hygroscopicity and RH. Therefore, very hygroscopic particles (i.e., sea salt) result in f(RH) uncertainty of ~14% at RH = 85%, while the total propagation error in f(RH = 85%) is ~20% by considering an absolute error of 1.5–2% in RH and 10% in the scattering coefficient (Zieger et al., 2013). Furthermore, the assumption of a dry aerosol at RH ≤ 40% instead of at RH = 0% might result in high (up to 25%) underestimation of the f(RH) for very hygroscopic aerosols, while for moderately hygroscopic aerosols this error does not exceed 10–15% (Titos et al., 2016).

Furthermore, meteorological variables including ambient temperature, RH, wind speed, and direction were measured during GVAX by an automatic weather station at the sampling site (Dumka et al., 2015a). In order to characterize the transport pathways of air masses arriving at Nainital and to detect the aerosol source regions responsible for changes in aerosol characteristics, 5-day backward trajectories at 500 m a.g.l. were obtained via the HYSPLIT4 model (Draxler and Rolph, 2016). The model version uses the GDAS (Global Data Assimilation System) meteorological data and includes profiles of vertical wind.

Although the GVAX campaign took place from June 2011 to March 2012, the light scattering enhancement factor is examined only during 1 November–13 December 2011 due to malfunctioning of the humidifier during January–March 2012 (Fig. 1). Furthermore, very high RH values at the reference Nephelometer were recorded during the humid and rainy summer monsoon (Fig. 1) resulting in large uncertainties in f(RH = 85%) at above 20–30%; therefore, the monsoon period was excluded from the analysis.

4. Results and discussion

4.1. Aerosol hygroscopicity

This section examines the temporal evolution and statistics of the f(RH) and γ values measured at 550 nm during 1st November–13th December 2011. Beyond these parameters, several other aerosol properties were also measured during GVAX campaign and are examined against enhancement factor; some of them are summarized in Figs. 2 and 3 for the $D_{10\ \mu m}$ and $D_{1\ \mu m}$, respectively. The σ_{sp} (550 nm) exhibited mean values of 322.66 ± 261.93 Mm^{-1} and 187.82 ± 144.25 Mm^{-1} for $D_{10\ \mu m}$ and $D_{1\ \mu m}$, respectively, while the corresponding values for σ_{ap} (530 nm) were found to be 18.16 ± 14.03 Mm^{-1} and 13.79 ± 9.84 Mm^{-1}, respectively during November–December 2011. Both σ_{sp} and σ_{ap} maximize during the first half of November (1−20) due to enhanced influence of transported agricultural biomass-burning plumes from northwestern IGP (Kaskaoutis et al., 2014b; Dumka et al., 2015a). During the same period there is also large variability for both hourly and daily values of the scattering and absorbing coefficients, which is attributed to changes in the emission rates, meteorological processes along the smoke-plume transport and boundary-layer dynamics over the measuring site, which resulted in a distinct diurnal pattern for the air pollutants with afternoon peaks (Dumka et al., 2015a). During the whole period, SSA at 550 μm ranged from 0.86 to 1.00 (mean of 0.94 ± 0.01) for $D_{10\ \mu m}$, while the corresponding values for $D_{1\ \mu m}$ were 0.87–1.00 (0.92 ± 0.02). During the period with enhanced σ_{sp} and σ_{ap} values, SSA remains at 0.92–0.94 for both size groups, indicating rather aging biomass-burning plumes transported over the Himalayan foothills after significant transformation processes (coagulation, condensation, and hydration) and atmospheric mixing with other aerosols (Dumka and Kaskaoutis, 2014). At the same period, the AAE is about 0.91 to 1.14 for the two size groups, suggesting less influence of aerosol from local biomass burning and much larger contribution from vehicles and industrial combustions (Zhang et al., 2015).

During the whole period, the hourly f(RH) values range between 1.00 and 1.56 (mean of 1.27 ± 0.12) and 1.00–1.64 (mean of 1.32 ± 0.14), for $D_{10\ \mu m}$ and $D_{1\ \mu m}$, respectively. On average, the f(RH) for $D_{1\ \mu m}$ is ~4% higher than that for $D_{10\ \mu m}$, indicating larger light-scattering enhancement factor for the fine particles. In addition, the range of f(RH = 85%) values is limited and both size groups exhibit a slight decreasing tendency towards December, corresponding to lower hygroscopicity. During the first half of November, when the open agricultural burning is still active over Punjab, northwest India, the f(RH = 85%) values remain at 1.34–1.39 for both size group, while a similar relatively small variability is observed for γ. However, during 20–25 November, there is a decreasing trend in f(RH = 85%) for both size groups, which is associated with small variation and rather low values for the σ_{sp} and σ_{sp} indicating the absence of thick aerosol plumes from the IGP. The increase in AAE may indicate enhanced contribution of re-suspended dust and/or BC aerosols from biomass combustions, which are more hydrophobic in nature and may reduce the f(RH = 85%) (Zieger et al., 2013; Titos et al., 2016; Shingler et al., 2016a, 2016b).

The slight decrease in f(RH) during December may be attributed to the different aerosol composition and the higher fraction of fresh local BC emissions for heating purposes. The scattering and absorption coefficients are significantly lower than those in November, and this may be attributed to the influence of meteorology and the fact that the measuring site usually remains above the polluted IGP layer (Dumka et al., 2015a). Therefore, the aerosol composition and atmospheric chemistry may be a little modified from the mostly aged plumes of mixture of carbonaceous aerosols and inorganic species (nitrates, sulfates, ammonium) from the industrialized IGP to the mostly local

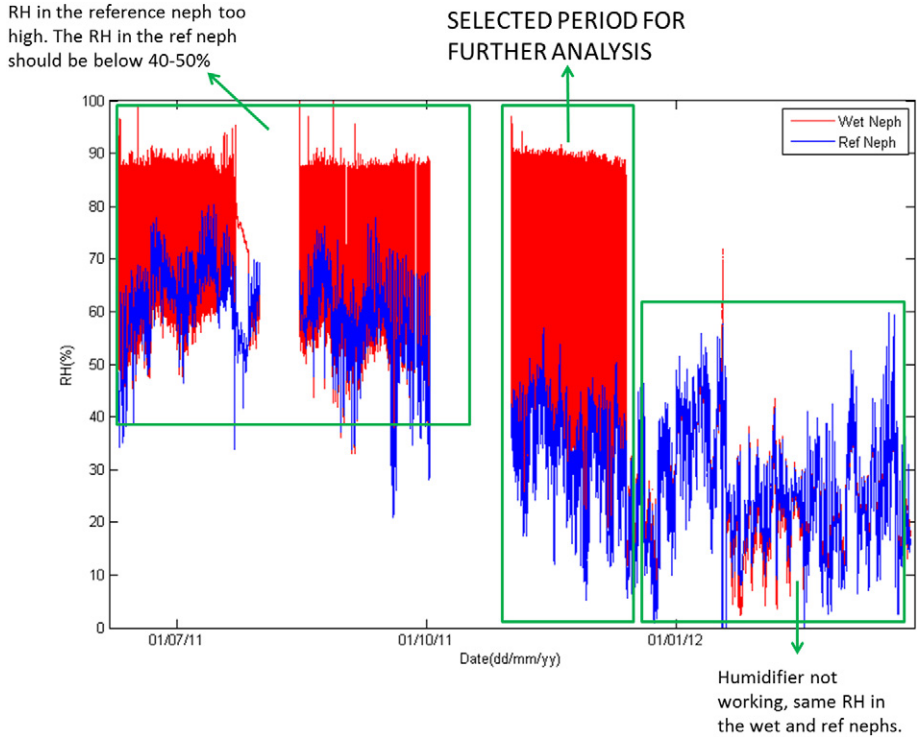

Fig. 1. Relative Humidity status of the dry and wet Nephelometer during the whole GVAX campaign at Nainital. The selected period for the analysis (1st November to 13th December) is shown.

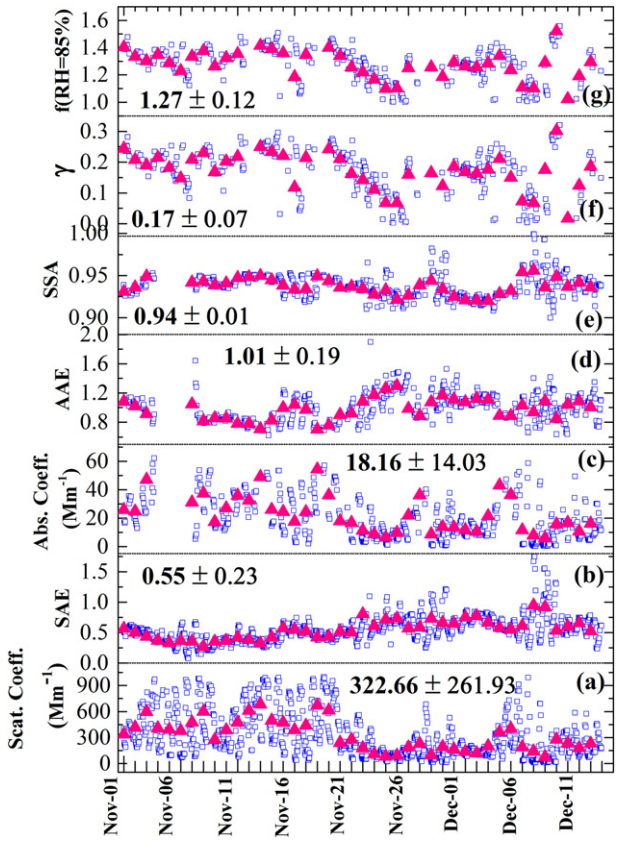

Fig. 2. Temporal evolution of the hourly (open squares) and daily-mean (magenta triangles) values of scattering coefficient (a), scattering Angstrom exponent (b), absorption coefficient (c), absorption Angstrom exponent (d), single scattering albedo (e), γ (f) and f(RH = 85%) (g) for $D_{10\ \mu m}$ at 550 nm at Nainital during 1st November–13th December. The absorption coefficient corresponds to 530 nm, the SAE to 450–700 nm and the AAE to 467–660 nm.

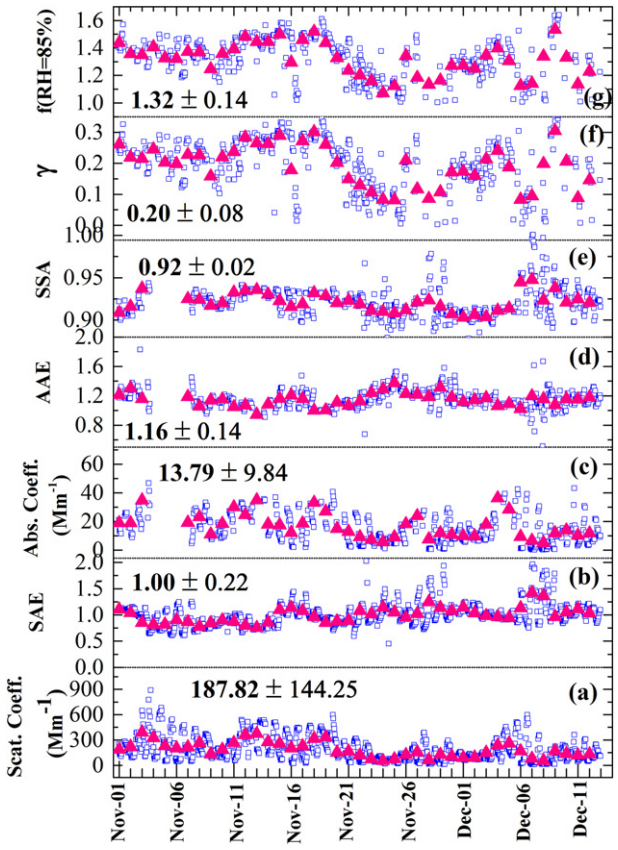

Fig. 3. Same as in Fig. 2, but for the $D_{1\ \mu m}$.

carbonaceous emissions, waste material and tree-leaves burning in several open fires in the roads for heating purposes as well as road dust resuspension, since no industries are located in Nainital. The aerosol mixture has a significant fraction (10–12%) of non-hygroscopic BC (soot aerosols) that suppresses or reduces the hygroscopicity (Lewis et al., 2009; Ram et al., 2010b). Due to much lower local emissions from a relative background Himalayan site in winter, the aerosol loading is less than that in November, and the aerosols seem to exhibit lower hygroscopicity. It is characteristic that both daily and hourly f(RH) values present a covariance between $D_{10\ \mu m}$ and $D_{1\ \mu m}$ with a correlation coefficient of r = 0.85 by considering the hourly f(RH = 85%) values, which indicates similar aerosol sources and composition for both size groups.

Contrary to our findings, Titos et al. (2014a) found larger f(RH = 80%) values of 1.8 ± 0.2 for PM_{10} against $PM_{1.0}$ (1.7 ± 0.2) in Cape Cod, east US coast under dominance of anthropogenic aerosols (Table 1). However, when marine clean conditions dominated over that location, the f(RH) was found to be larger (2.5 ± 0.6) for the $PM_{1.0}$ instead of PM_{10} (2.2 ± 0.2). Significant higher f(RH = 82%) values for $D_{1\ \mu m}$ (1.86) compared to $D_{10\ \mu m}$ were also reported by Carrico et al. (2000) for clean conditions in Sagres, Portugal, while polluted atmospheres over that site reduced f(RH) as well as the difference between $D_{1\ \mu m}$ and $D_{10\ \mu m}$ (f(RH) of 1.48 and 1.46, respectively), suggesting lower hygroscopicity (Table 1). Nessler et al. (2005) noticed that f(RH) was highly dependent on the mean particle diameter at a constant RH. Therefore, aerosol type and pollution levels seem to play a crucial role in determining the f(RH) values, which depend on the hygroscopic nature of aerosol and chemical composition (Carrico et al., 2000, 2003). It is worth noting that the f(RH) for marine aerosols shows a decrease under the influence of anthropogenic pollution plumes (McInnes et al., 1998; Gassó et al., 2000; Wang et al., 2007; Fierz-Schmidhauser et al., 2010b; Zieger et al., 2010; Titos et al., 2016). The estimated f(RH = 85%) values over Nainital are lower than those reported from several studies summarized in Table 1 (e.g., Carrico et al., 2003; Kim et al., 2006; Pan et al., 2009; Yan et al., 2009), as well as from those reported at polluted sites in eastern China, due to larger concentrations of hygroscopic (water-soluble) aerosols (i.e., nitrates, ammonium, sulfate) in China compared to IGP (Lu et al., 2011). In addition, dusty conditions resulted in lower f(RH = 80%) of 1.2 ± 0.02, compared to clean conditions f(RH = 80%) = 1.31 ± 0.03, and urban pollution with relative strong water-absorbing properties [f(RH = 80%) = 1.57 ± 0.02] (Pan et al., 2009). The dust particles in the coarse mode are mostly insoluble with f(RH = 80%) smaller than 1.1 (Li-Jones et al., 1998); however, they could become hygroscopic when coated with sulfate or other soluble inorganic aerosols during transportation and mixing (Perry et al., 2004; Shi et al., 2007). In this respect, an hygroscopic factor of f(RH = 80%) = 1.25 was observed for polluted dust in Ron Brown cruise during the Aerosol Characterization Experiment (ACE-Asia, April 2001) campaign (Carrico et al., 2003), while f(RH = 80%) values as high as 2.0 were found for dust particles transported over Korea (Kim et al., 2006). Kim et al. (2006) classified the f(RH = 80%) values according to the atmospheric conditions, founding f(RH = 80%) = 2.00 ± 0.27 during the dusty period, 2.75 during pollution plumes transported from China and 1.91 for local pollution. A study by Yan et al. (2009) at Shangdianzi, a baseline air pollution monitoring station in Beijing, showed that the f(RH = 80%) was 1.2 in clean air conditions and 1.48 during pollution episodes (opposite to the most of the studies summarized in Table 1). The f(RH) values during pollution outflows from Chinese (2.77 ± 0.37) and Korean sectors (1.91 ± 0.16) were much higher than those (1.46 ± 0.10) for anthropogenic aerosols in Europe during the ACE-2 campaign (Carrico et al., 2000) and higher than those (1.81 ± 0.37 to 2.30 ± 0.24) for

Table 1
Hygroscopic growth factors for different aerosol types over the globe.

Observational site	Predominant aerosol type	f(RH)	Reference
Nainital, India	Clean/background	$f(RH = 85\%) = 1.27$ in $D_{10\ \mu m}$ $f(RH = 85\%) = 1.32$ in $D_{1\ \mu m}$	Present study
Mace Head (Ireland)	Clean marine	$f(RH = 85\%) = 2.20$	Fierz-Schmidhauser et al. (2010c)
Cabauw (The Netherlands)	Maritime	$f(RH = 85\%) = 3.00$	Zieger et al. (2011)
Ny-Ålesund (Norway)	Artic	$f(RH = 85\%) = 3.50$	Zieger et al. (2010)
Southern Great Plains (OK, USA)	Continental	$f(RH = 85\%) = 1.83$	Sheridan et al. (2001)
Bondville (IL, USA)	Continental	$f(RH = 82.5\%) = 1.40–1.50$	Koloutsou-Vakakis et al. (2001)
Xin'An (China)	Dust dominated	$f(RH = 80\%) = 1.20$	Pan et al. (2009)
Jungfraujoch (Switzerland)	Dust dominated	$f(RH = 85\%) = 1.30$	Fierz-Schmidhauser et al. (2010b)
Southern Great Plains (OK, USA)	Dust dominated	$f(RH = 85\%) = 1.59$	Sheridan et al. (2001)
Granada (Spain)	Dust dominated	$f(RH = 85\%) = 1.30$	Titos et al. (2014b)
Beijing (China)	Urban	$f(RH = 80–85\%) = 1.26$	Yan et al. (2009)
Xin'An (China)	Urban pollution	$f(RH = 80\%) = 1.57$	Pan et al. (2009)
Granada (Spain)	Urban	$f(RH = 85\%) = 1.60$	Titos et al. (2014b)
Brazil	Biomass Burning	$f(RH = 80\%) = 1.16$ (1.01–1.51)	Kotchenruther and Hobbs (1998)
East Asia	Ocean	$f(RH = 82\%) = 2.45 \pm 0.27$	Carrico et al. (2003)
	Polluted	$f(RH = 82\%) = 2.22 \pm 0.20$	
	Sand	$f(RH = 82\%) = 1.18 \pm 0.20$	
	Volcano	$f(RH = 82\%) = 2.55 \pm 0.22$	
SDZ, Beijing a rural site	Relatively clean	$f(RH = 80 \pm 1\%) = 1.16$ $f(RH = 82 \pm 1\%) = 1.17$	Yan et al. (2009)
	Relatively polluted	$f(RH = 80 \pm 1\%) = 1.34$ $f(RH = 82 \pm 1\%) = 1.38$	
CAMS, Beijing an urban site	Relatively clean	$f(RH = 80 \pm 1\%) = 1.20$ $f(RH = 82 \pm 1\%) = 1.21$	Yan et al. (2009)
	Relatively polluted	$f(RH = 80 \pm 1\%) = 1.48$ $f(RH = 82 \pm 1\%) = 1.56$	
Cape Cod (MA, USA)	Anthropogenic	$f(RH = 80\%) = 1.80 \pm 0.20$ in PM_{10} $f(RH = 80\%) = 1.70 \pm 0.20$ in PM_1	Titos et al. (2014a)
	Marine	$f(RH = 80\%) = 2.20 \pm 0.30$ in PM_{10} $f(RH = 80\%) = 2.50 \pm 0.60$ in PM_1	
Mace Head (Ireland)	Polluted	$f(RH = 85\%) = 1.80$	Fierz-Schmidhauser et al. (2010b)
Indian Ocean (north)	Polluted	$f(RH = 82\%) = 1.55$ in $D_p < 1\ \mu m$	Sheridan et al. (2002)
Indian Ocean (central)	Polluted	$f(RH = 82\%) = 1.69$ in $D_p < 1\ \mu m$	Sheridan et al. (2002)
Indian Ocean (southern Hemisphere)	Clean marine	$f(RH = 82\%) = 2.07$ in $D_p < 1\ \mu m$	Sheridan et al. (2002)
Eastern North Atlantic Ocean	Polluted	$f(RH = 80\%) = 2.00$ in $D_p < 2.5\ \mu m$	Gassó et al. (2000)
	Clean	$f(RH = 80\%) = 2.50$ in $D_p < 2.5\ \mu m$	
Sagres, Portugal	Clean	$f(RH = 82\%) = 1.69$ in $D_p < 10\ \mu m$	Carrico et al. (2000)
	Polluted	$f(RH = 82\%) = 1.46$ in $D_p < 10\ \mu m$	
Sagres Portugal	Clean	$f(RH = 82\%) = 1.86$ in $D_p < 1\ \mu m$	Carrico et al. (2000)
	Polluted	$f(RH = 82\%) = 1.48$ in $D_p < 1\ \mu m$	
East Coast of US (TARFOX)	Urban/industrial	$f(RH = 80\%) = 1.81 \pm 0.37–2.30 \pm 0.24$	Kotchenruther et al. (1999)
Portugal (ACE-2)	Anthropogenic	$f(RH = 82\%) = 1.46 \pm 0.10$	Carrico et al. (2000)
Southern Africa (SAFARI 2000)	Biomass burning	$f(RH = 80\%) = 1.42 \pm 0.05–2.07 \pm 0.03$	Magi and Hobbs (2003)
Indian subcontinent (INDOEX)	Agricultural (burning/dust)	$f(RH = 85\%) = 1.58 \pm 0.21$	Sheridan et al. (2002)
East Asia (ACE-Asia)	Dust	$f(RH = 85\%) = 2.00 \pm 0.27$	Kim et al. (2006)
Gosan, Korea	Pollution (China)	$f(RH = 85\%) = 2.75 \pm 0.38$	Kim et al. (2006)
	Pollution (Korea)	$f(RH = 85\%) = 1.91 \pm 0.16$	
	Smoke (Biomass Burning)	$f(RH = 85\%) = 1.60 \pm 0.20$	
Cabauw (The Netherlands)	Maritime	$f(RH = 85\%) = 3.00$	Zieger et al. (2011)
Tropical Atlantic Ocean	Barbados, West Indies	$f(RH = 80\%) = 1.80$	Li-Jones et al. (1998)
SEAC^{4}RS campaign	Unites States (agricultural BB)	$f(RH = 80\%) = 1.08 \pm 0.13$	Shingler et al. (2016a)
	Unites States (wildfires BB)	$f(RH = 80\%) = 0.99 \pm 0.06$	
	Unites States (biogenic)	$f(RH = 80\%) = 1.41 \pm 0.13$	
	Unites States (marine)	$f(RH = 80\%) = 1.86 \pm 0.36$	
	United States (urban)	$f(RH = 80\%) = 1.64 \pm 0.19$	
	United States (background)	$f(RH = 80\%) = 1.41 \pm 0.20$	
	United States (free troposphere)	$f(RH = 80\%) = 1.36 \pm 0.27$	

urban/industrial aerosols over the east coast of United States during the Tropospheric Aerosol Radiative Forcing Observational Experiment (TARFOX) campaign (Kotchenruther et al., 1999). The f(RH) under smoke conditions (1.60 ± 0.20) was similar to that (1.58 ± 0.21) during the INDOEX campaign (Sheridan et al., 2002), but somewhat higher than that (1.16) during the smoke cloud and radiation Brazil (SCAR-B) campaign (Kotchenruther and Hobbs, 1998).

In synopsis, the f(RH) values at Nainital are generally lower than the most values summarized in Table 1. In general, aerosol hygroscopicity is mainly determined by the mass fraction of ammonium sulfate or nitrate in the accumulation mode (Chen et al., 2014). Moreover, it is seen that clean maritime aerosols have, in general, larger f(RH) values, while severe pollution, dust, and biomass-burning dominated atmospheres are characterized by lower particle hygroscopicity (Table 1). However, it

should be noted that significant differences may occur from place to place due to changes in atmospheric conditions and aerosol composition, while the RH level used for the determination plays also a crucial role leading to increased f(RH) for higher RH levels. In Nainital, the mostly steady atmospheric conditions dominated by slight northwesterly winds during late post-monsoon and winter and the absence of large changes in atmospheric circulation and air-mass transport (see Fig. 7), result in small variability in f(RH = 85%) for both size groups. The generally low f(RH = 85%) suggests the dominance of less hygroscopic aerosol at the local scale, while a small increase in f(RH) occurs when polluted air masses from the IGP reach the measuring site.

On the other hand, the γ values are in the range of 0.002–0.32 (mean of 0.17 ± 0.07) and 0.003–0.36 (mean of 0.20 ± 0.08) for $D_{10\ \mu m}$ and $D_{1\ \mu m}$, respectively during November–December 2011 (Figs. 2, 3). In agreement to f(RH), the temporal evolution of γ is consistent for both size groups, revealing the similar chemical composition and water uptake capability for sub-micron and super-micron particles, as justified by the strong correlation (r = 0.84) found between the γ values for $D_{10\ \mu m}$ and $D_{1\ \mu m}$. Titos et al. (2014a) reported mean γ values of ~0.5 for both $D_{1\ \mu m}$ and $D_{10\ \mu m}$ at Cape Cod, east US, but with relatively larger range for $D_{1\ \mu m}$ (0.1 to 1.1) compared to $D_{10\ \mu m}$ (0.2 and 0.9), which are higher than the current estimates. Therefore, the γ values over Nainital correspond to the dominance of more hydrophobic aerosols, mostly composed of soot and dust particles (Kotchenruther and Hobbs, 1998).

4.2. Frequency distribution of f(RH) and γ

Fig. 4(a–d) shows the frequency distributions of the f(RH) values for both size groups and for different groups of SAE and SSA. The SAE is a measure of the particle size with higher values corresponding to smaller aerosols, while SSA determines the aerosol absorption capability with lower values corresponding to more absorbing particles. The f(RH = 85%) value distributions show that, in general, the larger values (>1.3–1.4) are associated with increased frequency of SSA > 0.92 corresponding to more scattering aerosol types. In addition, the higher f(RH = 85%) is related to larger frequency for SAE values below 1.0, indicating aerosol particles of larger sizes. This characteristic is more pronounced in the case of $D_{1\ \mu m}$ particles, indicating that, in general, the larger and more scattering aerosols correspond to higher f(RH = 85%). This feature does not guarantee that such particles correspond to dust, but they may be also composed by nitrates, sulfates and organics, which are particles scattering in nature and may have SAE values below 1.0 after aging processes (Dumka et al., 2015a).

In contrast, aerosols that contain a higher fraction of absorbing particles (lower SSA) are, in general, less hygroscopic, since the frequency distribution is shifted towards lower f(RH) values (Fig. 4b, d), indicating that the soot aerosols, which also hold the larger fraction of the fine aerosols (SAE > 1.0) are the least hygroscopic at Nainital, which is in agreement with the literature (see Table 1 and Titos et al., 2016). The differences in f(RH) values for the two groups of SSA are generally low (f(RH = 85%) = 1.27 for SSA < 0.92 and f(RH = 85%) = 1.34 for SSA > 0.92 in the case of the $D_{1\ \mu m}$).

The frequency distributions of the γ values for $D_{10\ \mu m}$ and $D_{1\ \mu m}$ and for the different groups of SSA and SAE are shown in Fig. 5a–d. Despite the fact that there is not a clear shift for any group of the SAE and/or SSA values, the larger γ values are associated with higher frequency of SAE < 1.0 and SSA > 0.92, similarly to that observed for f(RH = 85%). More specifically, the γ values are slightly larger (0.21) for SAE < 1.0 compared to SAE > 1.0 (0.18), as well as for SSA > 0.92 (0.21) than for SSA < 0.92 (0.17), indicating that the larger and less absorbing particles tend to present higher rates of hygroscopicity in Nainital during November–December 2011. However, both f(RH) and γ do not exhibit a significant dependence on SSA and SAE values and the frequency distributions (Figs. 4 and 5) are rather complicated and mostly overlapped.

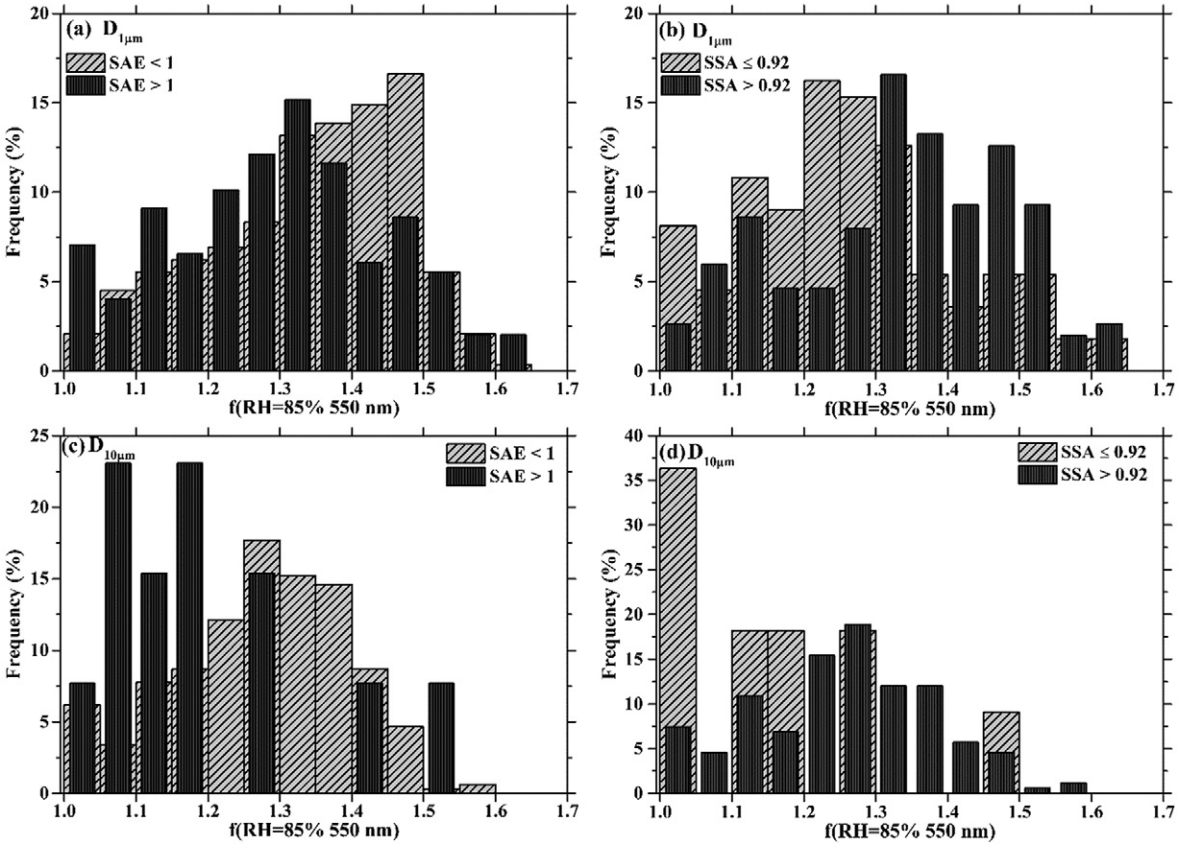

Fig. 4. Frequency distribution of the f(RH = 85%) values at 550 nm for different scattering Ångström exponent (SAE) and single scattering albedo (SSA) groups for $D_{1\ \mu m}$ and $D_{10\ \mu m}$ particle sizes.

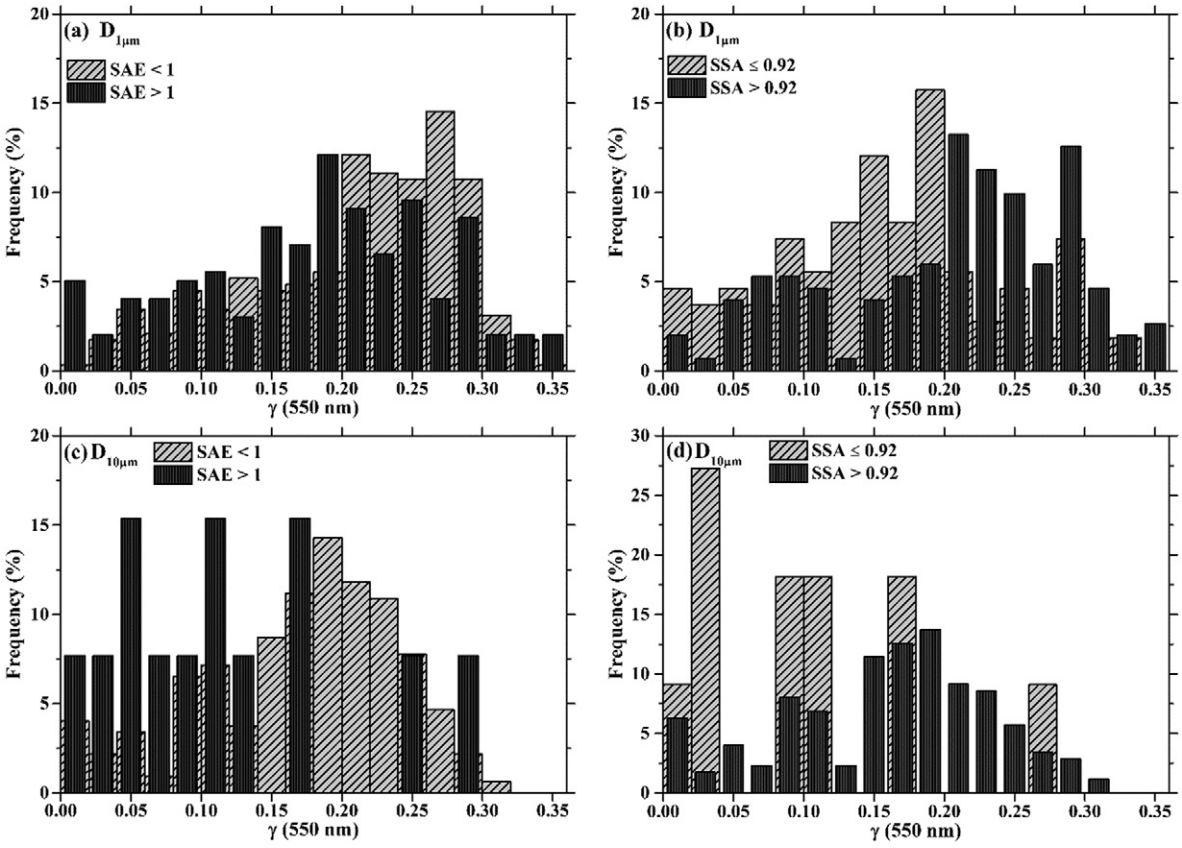

Fig. 5. Same as in Fig. 4, but for the fit parameter γ at 550 nm.

This suggests rather well-mixed atmospheric conditions with very difficult discrimination of the dominant aerosol species, especially in the case that aerosol samples and chemical analysis are not available. Therefore, the fine-mode aerosols dominated over the site in late post-monsoon and winter may suppress f(RH) in the case of BC and hydrophobic organics or enhance f(RH) in the case of WSOC and ammonium salts (Ram et al., 2010a, 2010b). The large fraction of non-hygroscopic carbonaceous aerosols suppresses the particle's hygroscopic growth (Carrico et al., 2005) and results in low f(RH) and γ values during November–December (Figs. 2 and 3). Therefore, the f(RH) and γ shift to lower values for the fine-mode soot aerosols (SAE < 1) than for coarse aerosols (SAE < 1) (Figs. 4 and 5). Titos et al. (2014b) reported that the frequency distribution of f(RH = 85%) was shifted to lower values for $SSA_{637} < 0.6$ and for SAE ($\alpha_{450-700}$) < 1, indicating that the more absorbing aerosols and/or the aerosols with larger coarse mode fraction were less hygroscopic in Granada urban area (Spain). The high relative contribution of absorbing particles might also explain the low hygroscopic enhancement [f(RH = 85%) = 1.32] observed in southeastern Spain (Titos et al., 2014b), while higher scattering enhancements were observed when fine particles [SAE-Ångström (dry, 450–700) values around 2] predominated (Titos et al., 2014b). Similarly to our results, the coarse aerosols were less hygroscopic over Granada, due to the large contribution of dust particles with low hygroscopicity over the site (Titos et al., 2014b). The larger particles ($D_{10\ \mu m}$) were found to be more absorbing compared to $D_{1\ \mu m}$ over Nainital during November–December 2011 (Manoharan et al., 2014; Dumka et al., 2015a); these particles are mostly composed of aged smoke coated with sulfate, ammonium, WSOC and nitrate from pollution plumes in IGP (Ram et al., 2010a, 2010b; Rajput et al., 2014; Rastogi et al., 2014). Titos et al. (2014a) proposed an exponential equation that successfully estimated the aerosol hygroscopicity as a function of SSA at Cape Cod, eastern USA. For SAE > 1, f(RH) was found to be similar in both size fractions, whereas f(RH) for $D_{1\ \mu m}$ increases when SAE < 1 (Titos et al., 2014a); a similar behavior was also referred for γ. In synopsis, the results showed that the particle size is very important for the hygroscopicity and can lead to compensation effects for f(RH); thus, fine and less hygroscopic aerosols may have similar (or even larger) values of f(RH) than larger and more hygroscopic aerosols (Zieger et al., 2010, 2013).

4.3. Role of wind speed and transported plumes on aerosol hygroscopicity

Fig. 6 shows the bivariate plots of f(RH = 85%) as a function of wind speed and direction for $D_{1\ \mu m}$ and $D_{10\ \mu m}$, aiming at identifying the sectors that mostly favor and/or associated with high aerosol hygroscopicity at Nainital. Previous studies during the GVAX campaign (Dumka et al., 2015a, 2015b) showed that the wind blows mostly from northwestern directions during late post-monsoon and winter and the air masses originating from these directions are associated with larger aerosol amounts (increase in scattering and absorption coefficients). The f(RH = 85%) bivariate plot for $D_{1\ \mu m}$ clearly shows that the highest particle hygroscopicity is associated with air masses coming from northwestern directions and under moderate-to-high wind speeds of 6–10 ms^{-1}, while the calm conditions and weak winds from the east are associated with very low values of f(RH = 85%). It is, therefore, concluded that the polluted air masses coming from the northwestern IGP contain more hygroscopic material, which is composed of a mixture of biomass burning and industrial pollution in this period (Ram et al., 2010a; Kaskaoutis et al., 2014b; Rastogi et al., 2014). In contrast, the local emissions accumulated over the site due to steady weather and the very shallow boundary layer (Dumka et al., 2015a) seem to be composed by hydrophobic aerosol (most likely large fractions of BC and/or re-suspended dust), as previous studies have found (Ram et al., 2010a; Manoharan et al., 2014). The f(RH = 85%) plot for the $D_{10\ \mu m}$, exhibits detectable differences from the previous case, since higher hygroscopicity is observed for air masses from northwestern directions but for lower wind speeds (3–6 ms^{-1}), as well as for eastern air masses of

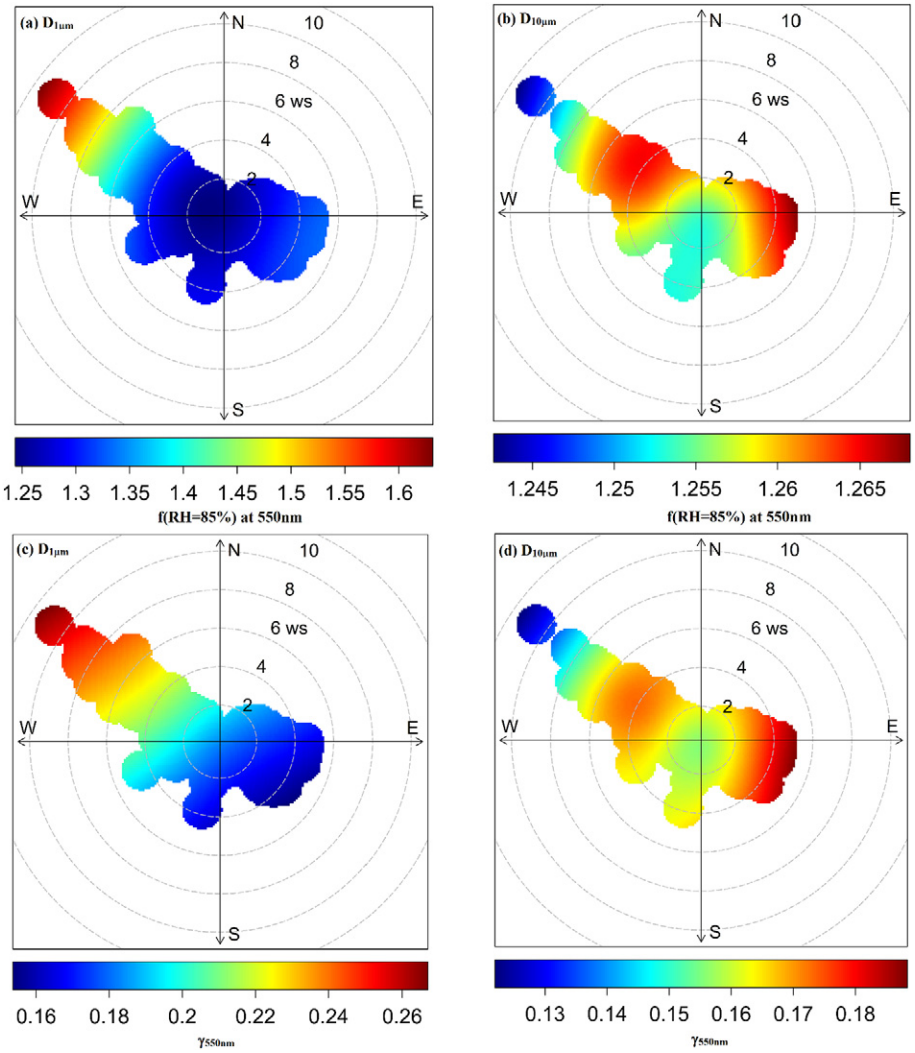

Fig. 6. Bivariate plots of f(RH = 85%) (upper row) and γ (below row) at 550 nm for $D_{1\ \mu m}$ and $D_{10\ \mu m}$.

3–5 ms^{-1}, which carry mostly clean-dry air from the Himalayas (see Fig. 7). The lower fraction of BC in the super-micron $D_{10\ \mu m}$ mass may influence the hygroscopicity, which, however, remains at the same levels [f(RH = 85%) = 1.25–1.3] as in the case of $D_{1\ \mu m}$ for calm conditions and eastern air masses. The respective bivariate plots for the γ coefficient (Fig. 6c, d) are mostly similar to those of f(RH = 85%) for the reasons described above.

Fig. 7 shows the 5-day backward trajectories obtained from HYSPLIT during the period November–December, which is color-coded by the daily-mean f(RH = 85%) value at Nainital. The fire spots derived from MODIS during the same period were also shown. Fig. 7 shows that the air masses reaching at Nainital from western/northwestern directions traverse the northwestern part of IGP, which suffers from a large number of agricultural fires in this season. Therefore, these air masses are able to carry a substantial amount of soot and carbonaceous aerosols, mixed with anthropogenic pollution mostly composed by organics, sulfate, nitrate and ammonium aerosol (Ram et al., 2010a; Rajput et al., 2014; Rastogi et al., 2014). In the vast majority of the cases the air masses were found to travel within the boundary layer (<2 km) over IGP, thus picking up biomass-burning aerosols and pollutants and carrying a mixture of hygroscopic and non-hygroscopic material over Nainital. The different kinds of burning material and phase of the fire may result in changes in the chemical composition of the fire emissions and, therefore, in different f(RH) values, as shown between smoke from Australian savannah fires and peat fires in Indonesia (Gras et al., 1999). This suggests that the fuel composition and the mixing processes play a major role in the f(RH) as shown in Fig. 7, since the air masses traversing the northwestern IGP, may have very different f(RH = 85%) values i.e., from 1.1 to 1.6. This consists of laboratory results (Hand et al., 2010) who found that the f(RH) ranged from 0.99 ± 0.08 to 1.81 ± 0.08 at RH = 80–85% depending on the fuel type. More specifically, the fuels with larger inorganic mass fractions and carbonaceous aerosols mixed with inorganic species exhibited higher f(RH) values. Therefore, the atmospheric mixing processes during the air-mass transport may also have an important contribution to the f(RH) at the measuring site. Furthermore, except of the fuel type, Day et al. (2006) highlighted the importance of the smoke aged processes in f(RH) values noticed that minute-old smoke is more hygroscopic than hour-old smoke, while changes in f(RH) values between areas affected by biomass burning may be also attributed to the hysteresis effect (Reid et al., 2005).

Based on the measured scattering coefficient, the whole dataset of aerosol properties was classified into three groups (i) clean/background, (ii) polluted/haze and (iii) unclassified using the thresholds of the scattering coefficient for $D_{1\ \mu m}$ and $D_{10\ \mu m}$ (<mean − 1 standard deviation for the clean and >mean + 1 standard deviation for the polluted). The datasets that do not fall into these groups are considered as unclassified. The mean f(RH) = 85% values at 550 nm for the background and polluted cases were found to be 1.19 ± 0.09 and 1.44 ± 0.06, respectively for $D_{1\ \mu m}$, while the respective values for $D_{10\ \mu m}$ were 1.17 ± 0.08 and 1.37 ± 0.05 (Table 2). Higher γ values under

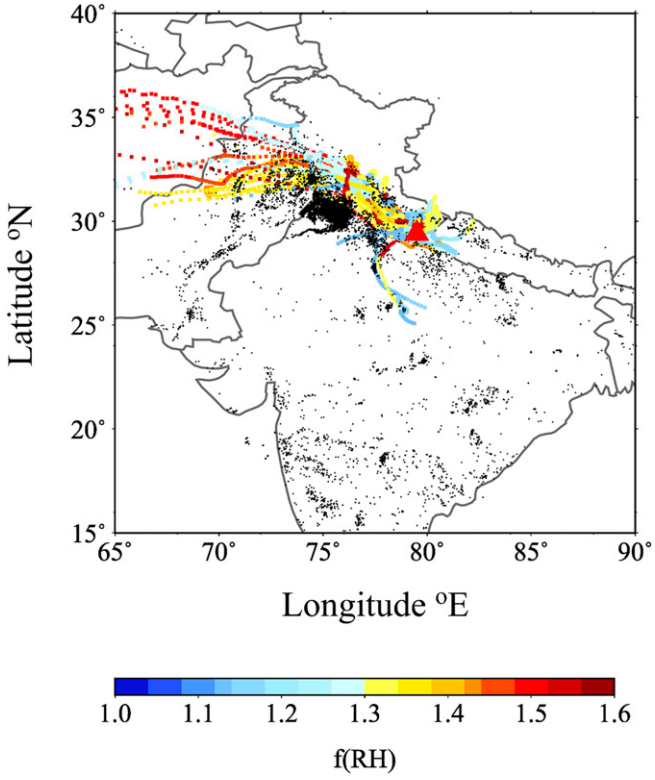

Fig. 7. Five day air-mass back trajectories color coded by the f(RH = 85%) at the arriving day at Nainital. The black dots show the MODIS fire counts during November–December 2011.

more aerosol-laden conditions were also found (Table 2), opposite to the most of the studies summarized in Table 1. The SSA values are similar for both groups, while significantly lower SAE values were found under polluted conditions, indicating the dominance of coarse-mode or aged aerosols. Contrary to our results, larger values of f(RH) were observed at the arctic clean-maritime site of Ny-Ålesund, compared to more polluted European sites (Zieger et al., 2010, 2013). However, the clean air masses over Nainital coming from the Himalayas are continental and dry (without sea salt or marine particles) and, therefore, much less hygroscopic in nature than the Arctic air masses. Similarly to Nainital, Kotchenruther et al. (1999) reported higher f(RH) values for polluted than for clean maritime air masses due to enriched sulfate aerosols from anthropogenic emissions. Furthermore, slightly higher f(RH) values for polluted continental aerosols rather than clean air masses were reported in China (Yan et al., 2009; Chen et al., 2014).

4.4. Relationship between f(RH) and γ with aerosol properties

For better understanding the sensitivity of f(RH) on aerosol properties, correlations between f(RH = 85%) and main in-situ aerosol variables (σ_{sp}, σ_{ap} SAE, SSA) have been performed at several sites over the globe (e.g., Doherty et al., 2005; Nessler et al., 2005; Titos et al., 2014a). In this respect, Fig. 8 shows the correlation between the f(RH = 85%) and the scattering coefficient as a function of SSA (top panels) and SAE (bottom panels) for both $D_{10\ \mu m}$ and $D_{1\ \mu m}$, while the respective correlations between σ_{ap} and f(RH = 85%) are shown in Fig. 9.

The analysis shows that regardless of the particle size, the f(RH) tends to increase for polluted episodes (high σ_{sp} values) than for low σ_{sp}, as already found in the previous analysis. Despite the large scatter of the data points, the increase of f(RH = 85%) with σ_{sp} and σ_{ap} was found to be statistically significant at 95% confidence level. In general similarity with the current findings, f(RH) was distinctly higher for polluted cases than for clean atmospheres at a specific RH in China (Chen et al., 2014). The current graphical representation does not show a tendency between f(RH = 85%) and particle size expressed via SAE (Fig. 8), but a slight negative correlation associated with 2.7% (6.85%) of the variance was found between f(RH = 85%) and SAE for the $D_{1\ \mu m}$ ($D_{10\ \mu m}$). Similarly, the dependence of f(RH = 85%) on SSA is rather small revealing a slightly increasing trend, but very low coefficients of determination ($R^2 = 0.01$ for the $D_{1\ \mu m}$ and $D_{10\ \mu m}$) rendering it as statistically insignificant at 95% confidence level. However, f(RH = 85%) values above ~1.4 are mostly associated with higher SSA and lower SAE values and this is more pronounced for the $D_{1\ \mu m}$.

It should be also noted that the changes in the aerosol scattering coefficient with RH drive changes in SSA, SAE or backscatter coefficient. Titos et al. (2014a) found that the larger and more scattering particles (lower SAE and higher SSA) had larger scattering enhancement at the eastern US coast, which is in consistency with our results (Fig. 8). Similarly, they reported a moderate correlation between f(RH) and SSA with R^2 in the range of 0.2–0.3 and the generally low correlation between f(RH) and Ångström exponent (Titos et al., 2014b). Furthermore, it was found (Doherty et al., 2005) that the f(RH) increases with enhanced contribution of sub-micrometer particles to the scattering coefficient.

Analogous features are observed between f(RH) and σ_{ap} (Fig. 9), indicating that the f(RH = 85%) increases with increase in absorption coefficient (turbid atmospheres) for both size groups, but remains mostly independent from the AAE, although a slight decreasing curve was found between them. Fig. 10 shows the dependence of f(RH = 85%) on N_{CCN} at the saturation level 0.75–0.78%, as a function of the activation ratio (AR). A comprehensive investigation of N_{CCN} and examination between aerosol and clouds during the GVAX campaign were performed by Dumka et al. (2015b) and Gogoi et al. (2015). The larger f(RH = 85%) values are associated with higher N_{CCN}, with their between correlation to be found statistically significant for the $D_{1\ \mu m}$, but not for the $D_{10\ \mu m}$. This indicates that more hygroscopic particles grow to larger sizes (at fixed RH), also exhibiting greater CCN activity, thus influencing cloud microphysical properties and the hydrologic cycle (Shingler et al., 2016a). Furthermore, the low dependence of f(RH) on AR is shown, although the majority of the low AR values correspond to lower f(RH = 85%). Dumka et al. (2015b) found a higher increasing trend of N_{CCN} against saturation (s) in winter compared to the summer monsoon, while for S > 0.45% there was no new N_{CCN} formation in summer in contrast to that observed in winter. Therefore, the increasing trend between f(RH) = 85% and N_{CCN} indicates more hygroscopic aerosols and larger N_{CCN} formation for the high f(RH = 85%).

Table 2
Aerosol properties at Nainital in clean/background, polluted/turbid and unclassified conditions during 1st November to 13th December 2011.

Parameters	$D_{1\ \mu m}$			$D_{10\ \mu m}$		
	Clean/background	Polluted/turbid	Unclassified	Clean/background	Polluted/turbid	Unclassified
$\sigma_{sp(550\ nm)}$	72.64 ± 15.11	350.04 ± 29.88	185.39 ± 53.08	111.22 ± 24.05	629.93 ± 37.74	303.60 ± 119.53
$\sigma_{ap(530\ nm)}$	7.60 ± 1.81	30.97 ± 4.76	17.23 ± 6.81	8.87 ± 1.78	42.83 ± 8.63	21.29 ± 9.32
$SAE_{(450–700\ nm)}$	1.18 ± 0.15	0.84 ± 0.07	0.98 ± 0.11	0.75 ± 0.11	0.38 ± 0.07	0.55 ± 0.14
$AAE_{(467–660\ nm)}$	1.21 ± 0.09	1.04 ± 0.08	1.15 ± 0.07	1.14 ± 0.13	0.78 ± 0.08	0.99 ± 0.11
$SSA_{(550\ nm)}$	0.92 ± 0.01	0.93 ± 0.00	0.92 ± 0.01	0.93 ± 0.01	0.95 ± 0.00	0.94 ± 0.01
$f_{(RH\ =\ 85\%;\ 550\ nm)}$	1.19 ± 0.09	1.44 ± 0.06	1.32 ± 0.11	1.17 ± 0.08	1.37 ± 0.05	1.28 ± 0.09
$\gamma_{(550\ nm)}$	0.12 ± 0.05	0.26 ± 0.03	0.20 ± 0.06	0.11 ± 0.05	0.23 ± 0.03	0.18 ± 0.05

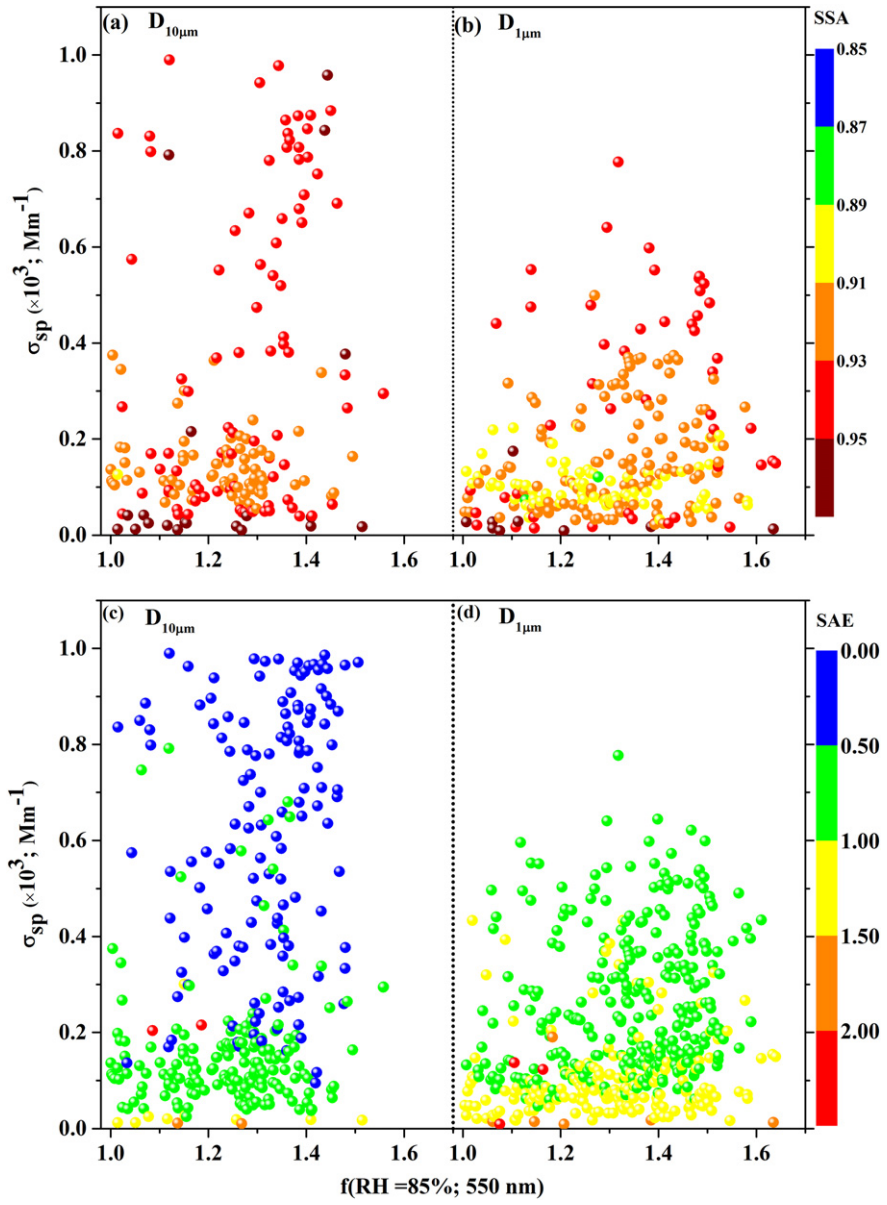

Fig. 8. Scatter plot between f(RH = 85%) and scattering coefficient as a function of single scattering albedo (a, b) and scattering Angstrom exponent (c, d) for the $D_{10\ \mu m}$ and $D_{1\ \mu m}$ size groups.

4.5. Unexplored issues, challenges, and future work

Nainital is a high-altitude site with low local emissions but strongly affected by transported aerosol plumes of different origin and composition i.e., dust storms, agricultural biomass burning, industrial and vehicle pollution, which result in large differences in the aerosol particle hygroscopicity. On the other hand, the aerosol hygroscopicity depends on the optical aerosol properties, aerosol chemistry, size distribution, and meteorology. The present study is the first that examines the aerosol hygroscopicity over Nainital presenting some preliminary results during the GVAX campaign. However, several issues have remained unexplored due to lack of the appropriate instrumentation during the campaign, like Hygroscopic Tandem Differential Mobility Analyser (HTDMA) measurements for estimating the hygroscopic growth factor, chemical composition analysis for identifying the most hygroscopic components and analytic aerosol size distribution that would have given a view of the hygroscopic growth as a function of the particle size (Shingler et al., 2016b).

The particle size and the chemical composition play the major role in determining the aerosol hygroscopic properties. Lack of chemical measurements during the campaign period constitutes a real challenge for investigating its effect on the value of f(RH). In this respect, Zieger et al. (2014) found that the magnitude of f(RH) was correlated with the inorganic mass fraction and Garland et al. (2007) reported a linear variation of the f(RH = 80%) with the organic/inorganic content. The larger organic carbon (OC) fraction results in decrease of f(RH) (Malm et al., 2005), which has been justified over Granada, Spain where a significant ($R^2 = 0.78$) decreasing trend of f(RH) with the particulate organic matter (POM) fraction was observed (Titos et al., 2014b). Similarly, Quinn et al. (2005) found lower POM contribution and higher hygroscopicity for the aged rather than freshly emitted aerosols. Similarly, Pagels et al. (2009) reported that the transformation of soot particles to spherical droplets can be achieved after several hours from the initial emissions and under atmospheric aging processes. Therefore, during November–December with the enhanced smoke concentrations over Nainital, the increasing RH and mass fraction of condensed soluble

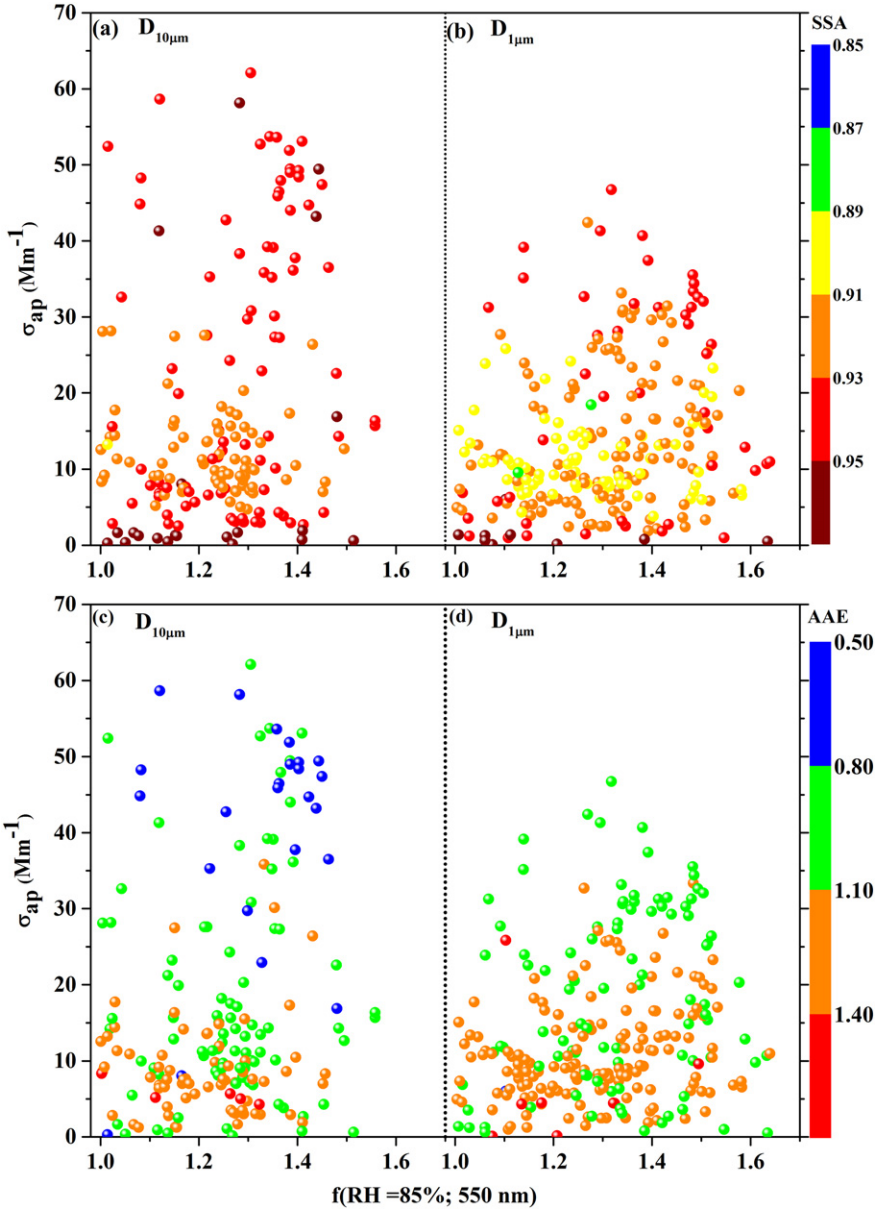

Fig. 9. Same as in Fig. 8, but between f(RH = 85%) and absorption coefficient as a function of SSA and absorption Ansgtrom exponent.

materials onto fresh soot result in drastic changes in the light scattering and absorption coefficients of the soot aerosol (Khalizov et al., 2009; Pagels et al., 2009). As a consequence, the generally low SAE values associated with high absorption for $D_{10\ \mu m}$ particles in November 2011 (Manoharan et al., 2014; Dumka et al., 2015a) may be partly attributed to the hygroscopic growth of the soot particles. Finally, the simulation of f(RH) values via the Mie theory, as performed in previous studies (e.g., Adam et al., 2012; Zieger et al., 2013), requires additional measurements of particle number size distribution via Scanning Mobility Particle Sizer (SMPS) and Optical Particle Counter (OPC), of hygroscopic growth factor via HTDMA and of chemical composition via PM samples that were not available during the GVAX campaign. With the appropriate datasets f(RH) could be also used to estimate the hygroscopic growth (κ) values using measured size distribution and the Mie theory (Zieger et al., 2010; Shingler et al., 2016a).

Accurate estimates of the changes in aerosol optical and physical properties due to water uptake are also crucial for radiative forcing studies (Zieger et al., 2013; Titos et al., 2014b), especially for organic aerosols, soot and dust (Malm and Kreidenweis, 1997; Mircea et al., 2005) that dominate over Nainital. The increase of RH will cause changes in the intensive aerosol properties (i.e., SSA, SAE, AAE, etc) as well, resulting in dependence of aerosol radiative forcing (ARF) on RH. In this respect, Fierz-Schmidhauser et al. (2010c) reported a decrease of ~20% in the backscatter fraction and an increase of 1%–5% in SSA at RH = 85% compared to dry conditions. Furthermore, Titos et al. (2014b) found that the ARF efficiency changed from −13 W m^{-2} at dry conditions to −17 W m^{-2} at RH = 85%, underlying the importance of the aerosol hygroscopic effect on ARF. Consequently, aerosol hygroscopic growth will have an immense impact on aerosol optical properties and cloud droplet activation (Deng et al., 2011; Chen et al., 2014), as well as to cloud formation and precipitation over the Himalayan foothills. New research campaigns in the future or systematic measurements with new instrumentation over the site will provide the basic dataset for examining the hygroscopic growth factor from a new perspective, as was performed at several places over the globe.

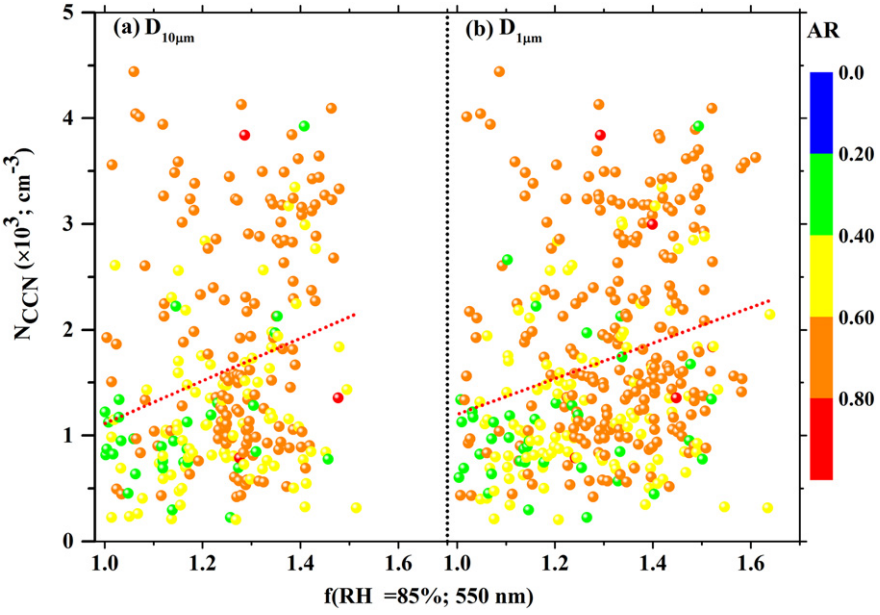

Fig. 10. Correlation between the f(RH = 85%) and the cloud condensation nuclei concentration (N_{CCN}) as a function of the activation ratio (AR) for $D_{10\ \mu m}$ and $D_{1\ \mu m}$ size goups.

5. Conclusions

This paper examined the aerosol hygroscopicity for the first time at Nainital, central Indian Himalayas during 1st November–13th December 2011 in the framework of the GVAX campaign. The f(RH) quantifies the change in the particle light-scattering coefficient due to water uptake and is especially important for several atmospheric issues. The f(RH = 85%) values were estimated by means of two Nephelometer, one working at dry conditions and one at high RH (80–85%) connected with a humidifier. Furthermore, several other aerosol parameters, like scattering coefficient, absorption coefficient, N_{CCN} and their intensive properties such as SSA, SAE, AAE were estimated via multiple instrumentations during the campaign and were examined against f(RH = 85%) values. The main findings are summarized as follows:

1. The f(RH = 85%) values show significant daily variability due to different sources, aerosol types and chemical composition. During the studied period, the f(RH = 85%) values in $D_{10\ \mu m}$ and $D_{1\ \mu m}$ particle groups were found to be 1.27 ± 0.12 and 1.32 ± 0.14, respectively, while the corresponding fit parameters γ were 0.17 ± 0.07 and 0.20 ± 0.08 for $D_{10\ \mu m}$ and $D_{1\ \mu m}$, respectively, denoting larger scattering enhancement in the fine mode.
2. The distribution of the f(RH = 85%) and γ values did not show a strong dependence on the particle size (defined via SAE) and on the absorption capability (defined via SSA) for the $D_{10\ \mu m}$ and $D_{1\ \mu m}$ particle groups. However, the high f(RH = 85%) values were associated with the larger fraction of SAE < 1 and SSA > 0.92. This indicates that the coarser and less absorbing aerosols were more hygroscopic during November–December, a period that mostly dominated by biomass-burning conditions.
3. The air masses reaching Nainital traversed the areas suffering from agricultural biomass burning in northwestern India and the large (from 1.00 to 1.56) variability in f(RH = 85%) indicated mixing with polluted air masses over the Ganges Valley and dependence of aerosol hygroscopicity and light-scattering enhancement on the phase of the fire and composition of the burning material.
4. The significant dependence of f(RH = 85%) on the scattering and absorption coefficients indicated higher aerosol hygroscopicity under polluted/haze atmospheres over the central Himalayas. These polluted air masses seem to be composed of mixing of agricultural biomass burning and urban/industrial pollution originating from the Ganges Valley. The local air masses during winter in Nainital were found to be less hygroscopic. Furthermore, higher f(RH = 85%) values were associated with increased N_{CCN} implying higher possibility for the formation of cloud condensation nuclei.

Acknowledgement

This work was carried out as a part of GVAX (https://www.arm.gov/sites/amf/pgh/) campaign in the joint collaboration among US Department of Energy (DoE) and Indian Space Research Organization (ISRO), Indian Institute of Science, Bangalore and ARIES Nainital India. We thanks, Director ARIES and Dr. Wand R Ferrell for providing the necessary support. We are grateful to the technical staff of ARM for providing the valuable archival data (http://www.archive.arm.gov/). We thank the NOAA Air Resources Laboratory for the provision of the HYSPLIT transport and dispersion model used in this study. The authors are thankful to Prof. L. Alados-Arboledas and Dr. Gloria Titos for insightful comments and suggestions, which helped us significantly in improving the scientific quality of the manuscript.

References

Adam, M., Putaud, J.P., Martins dos Santos, S., Dell'Acqua, A., Gruening, C., 2012. Aerosol hygroscopicity at a regional background site (Ispra) in Northern Italy. Atmos. Chem. Phys. 12, 5703–5717.

Anderson, T.L., Ogren, J.A., 1998. Determining aerosol radiative properties using the TSI 3563 integrating Nephelometer. Aerosol Sci. Technol. 29, 57–69.

Anderson, T.L., Covert, D.S., Marshall, S.F., Laucks, M.L., et al., 1996. Performance characteristics of a high-sensitivity, three-wavelength, total scatter/backscatter Nephelometer. J. Atmos. Ocean. Technol. 13, 967–986.

Carrico, C.M., Rood, M.J., Ogren, J.A., Neusüb, C., Wiedensohler, A., Heintzenberg, J., 2000. Aerosol optical properties at Sagres, Portugal during ACE-2. Tellus 52, 694–715.

Carrico, C.M., Kus, P., Rood, M.J., Quinn, P.K., Bates, T.S., 2003. Mixtures of pollution, dust, sea salt, and volcanic aerosol during ACE-Asia: radiative properties as a function of relative humidity. J. Geophys. Res. 108:8650. http://dx.doi.org/10.1029/2003JD003405.

Carrico, C.M., Kreidenweis, S.M., Malm, W.C., Day, D.E., Lee, T., Carrillo, J., McMeeking, G.R., Collett, J.L., 2005. Hygroscopic growth behavior of a carbon-dominated aerosol in Yosemite National Park. Atmos. Environ. 39, 1394–1404.

Carrico, C.M., Petters, M.D., Kreidenweis, S.M., Collett, J.L., Engling, G., Malm, W.C., 2008. Aerosol hygroscopicity and cloud droplet activation of extracts of filters from biomass burning experiments. J. Geophys. Res. 113, D08206. http://dx.doi.org/10.1029/2007JD009274.

Chen, J., Zhao, C.S., Ma, N., Yan, P., 2014. Aerosol hygroscopicity parameter derived from the light scattering enhancement factor measurements in the North China Plain. Atmos. Chem. Phys. 14, 8105–8118.

Clarke, A.D., Howell, S., Quinn, P.K., Bates, T.S., Ogren, J.A., Andrews, E., Jefferson, A., Massling, A., Mayol-Bracero, O., Maring, H., Savoie, D., Cass, G., 2002. INDOEX aerosol: a comparison and summary of chemical, microphysical, and optical properties observed from land, ship, and aircraft. J. Geophys. Res. 107:8033. http://dx.doi.org/10.1029/2001JD000572.

Day, D.E., Hand, J.L., Carrico, C.M., Engling, G., Malm, W.C., 2006. Humidification factors from laboratory studies of fresh smoke from biomass fuels. J. Geophys. Res. 111, D22202 (doi: 22210.21029/22006JD007221).

Deng, Z.Z., Zhao, C.S., Ma, N., Liu, P.F., Ran, L., Xu, W.Y., Chen, J., Liang, Z., Liang, S., Huang, M.Y., Ma, X.C., Zhang, Q., Quan, J.N., Yan, P., Henning, S., Mildenberger, K., Sommerhage, E., Schafer, M., Stratmann, F., Wiedensohler, A., 2011. Size-resolved and bulk activation properties of aerosols in the North China Plain. Atmos. Chem. Phys. 11, 3835–3846.

Dey, S., Di Girolamo, L., 2010. A climatology of aerosol optical and microphysical properties over the Indian subcontinent from 9 years (2000–2008) of multiangle imaging spectro-radiometer (MISR) data. J. Geophys. Res. 115, D15204. http://dx.doi.org/10.1029/2009JD013395.

Doherty, S.J., Quinn, P.K., Jefferson, A., Carrico, C.M., Anderson, T.L., Hegg, D., 2005. A comparison and summary of aerosol optical properties as observed in situ from aircraft, ship, and land during ACE-Asia. J. Geophys. Res. 110, D04201.

Draxler, R.R., Rolph, G.D., 2016. HYSPLIT (HYbrid Single-particle Lagrangian Integrated Trajectory) Model Access via NOAA ARL READY. NOAA Air Resources Laboratory, Silver Spring, MD (Website. http://ready.arl.noaa.gov/HYSPLIT.php).

Dumka, U.C., Kaskaoutis, D.G., 2014. In-situ measurements of aerosol properties and estimates of radiative forcing efficiency over Gangetic-Himalayan region during the GVAX field campaign. Atmos. Environ. 94:96–105. http://dx.doi.org/10.1016/j.atmosenv.2014.05.021.

Dumka, U.C., Kaskaoutis, D.G., Srivastava, M.K., Devara, P.C.S., 2015a. Scattering and absorption properties of near-surface aerosol over Gangetic-Himalayan region: the role of boundary layer dynamics and long-range transport. Atmos. Chem. Phys. 14, 21101–21148.

Dumka, U.C., Bhattu, Deepika, Tripathi, S.N., Kaskaoutis, D.G., Madhavan, B.L., 2015b. Seasonal inhomogeneity in cloud precursors over Gangetic Himalayan region during GVAX campaign. Atmos. Res.

Esteve, A.R., Ogren, J.A., Sheridan, P.J., Andrews, E., Holben, B.N., Utrillas, M.P., 2012. Sources of discrepancy between aerosol optical depths obtained from AERONET and in-situ aircraft profiles. Atmos. Chem. Phys. 12, 2987–3003.

Fierz-Schmidhauser, R., Zieger, P., Wehrle, G., Jefferson, A., Ogren, J.A., Baltensperger, U., Weingartner, E., 2010a. Measurement of relative humidity dependent light scattering of aerosols. Atmos. Meas. Tech. 3:39–50. http://dx.doi.org/10.5194/amt-3-39-2010.

Fierz-Schmidhauser, R., Zieger, P., Gysel, M., Kammermann, L., DeCarlo, P.F., Baltensperger, U., Weingartner, E., 2010b. Measured and predicted aerosol light scattering enhancement factors at the high alpine site Jungfraujoch. Atmos. Chem. Phys. 10:2319–2333. http://dx.doi.org/10.5194/acp-10-2319-2010.

Fierz-Schmidhauser, R., Zieger, P., Vaishya, A., Monahan, C., Bialek, J., O'Dowd, C.D., Jennings, S.G., Baltensperger, U., Weingartner, E., 2010c. Light scattering enhancement factors in the marine boundary layer (Mace Head, Ireland). J. Geophys. Res. 115, D20204. http://dx.doi.org/10.1029/2009JD013755.

Garland, R.M., Ravishankara, A.R., Lovejoy, E.R., Tolbert, M.A., Baynard, T., 2007. Parameterization for the relative humidity dependence of light extinction: organic-ammonium sulfate aerosol. J. Geophys. Res. 112, D19303. http://dx.doi.org/10.1029/2006JD008179.

Gassó, S., Hegg, D.A., Covert, D.S., Collins, D., Noone, K.J., Öström, E., Schmid, B., Russell, P.B., Livingston, J.M., Durkee, P.A., Jonsson, H., 2000. Influence of humidity on the aerosol scattering coefficient and its effect on the upwelling radiance during ACE-2. Tellus 52, 546–567.

Gautam, R., Hsu, N.C., Lau, K.-M., Kafatos, M., 2009. Aerosol and rainfall variability over the Indian monsoon region: distributions, trends and coupling. Ann. Geophys. 29, 3691–3703.

Gogoi, M.M., Babu, S.S., Jayachandran, V., Moorthy, K.K., Satheesh, S.K., Naja, M., Kotamarthi, V.R., 2015. Optical properties and CCN activity of aerosols in a high-altitude Himalayan environment: results from RAWEX-GVAX. J. Geophys. Res. 120: 2453–2469. http://dx.doi.org/10.1002/2014JD022966.

Gras, J.L., Jensen, J.B., Okada, K., Ikegami, M., Zaizen, Y., Makino, Y., 1999. Some optical properties of smoke aerosol in Indonesia and Tropical Australia. Geophys. Res. Lett. 26 (10), 1393–1396.

Hand, J.L., Day, D.E., McMeeking, G.M., Levin, E.J.T., Carrico, C.M., Kreidenweis, S.M., Malm, W.C., Laskin, A., Desyaterik, Y., 2010. Measured and modeled humidification factors of fresh smoke particles from biomass burning: role of inorganic constituents. Atmos. Chem. Phys. Discuss. 10:4225–4269. http://dx.doi.org/10.5194/acpd-10-4225-2010.

Hänel, G., Zankl, B., 1979. Aerosol size and relative humidity: water uptake by mixtures of salts. Tellus 31, 478–486.

Jefferson, A., 2011. Aerosol Observing System (AOS) Handbook. U.S. Department of Energy, DOE/SC- ARM/TR-014 available at. http://www.arm.gov/publications/tech_reports/handbooks/aos_handbook.pdf (last access: January 2014).

Kambezidis, H.D., Kaskaoutis, D.G., Kharol, S.K., Moorthy, K.K., Satheesh, S.K., Kalapureddy, M.C.R., Badarinath, K.V.S., Sharma, A.R., Wild, M., 2012. Multi-decadal variation of the net downward shortwave radiation over south Asia: the solar dimming effect. Atmos. Environ. 50, 360–372.

Kaskaoutis, D.G., Houssos, E.E., Goto, D., Bartzokas, A., Nastos, P.T., Sinha, P.R., Kharol, S.K., Kosmopoulos, P.G., Singh, R.P., Takemura, T., 2014a. Synoptic weather conditions and aerosol episodes over Indo-Gangetic Plains, India. Clim. Dyn. 43, 2313–2331.

Kaskaoutis, D.G., Kumar, S., Sharma, D., Singh, R.P., Kharol, S.K., Sharma, M., Singh, A.K., Singh, S., Atinderpal, Singh, Singh, D., 2014b. Effects of crop residue burning on aerosol properties, plume characteristics and long-range transport over northern India. J. Geophys. Res. http://dx.doi.org/10.1002/2013JD021357.

Khalizov, A.F., Zhang, R., Zhang, D., Xue, H., Pagels, J., McMurry, P.H., 2009. Formation of highly hygroscopic soot aerosols upon internal mixing with sulfuric acid vapor. J. Geophys. Res. 114:D5. http://dx.doi.org/10.1029/2008JD010595.

Kim, J., Yoon, Soon Chang, Jefferson, Anne, Sang-Woo, Kim, 2006. Aerosol hygroscopic properties during Asian dust, pollution, and biomass burning episodes at Gosan, Korea in April 2001. Atmos. Environ. 40 (8), 1550–1560.

Koloutsou-Vakakis, S., Carrico, C.M., Kus, P., Rood, M.J., Li, Z., Shrestha, R., Ogren, J.A., Chow, J.C., Watson, G., 2001. Aerosol properties at a midlatitude Northern Hemisphere continental site. J. Geophys. Res. 106, 3019–3032.

Kotchenruther, R.A., Hobbs, P.V., 1998. Humidification factors of aerosols from biomass burning in Brazil. J. Geophys. Res. 103 (D24), 32081–32089.

Kotchenruther, R.A., Hobbs, P.V., Hegg, D.A., 1999. Humidification factors for atmospheric aerosols off the mid-Atlantic coast of the United States. J. Geophys. Res. 104, 2239–2251.

Lawrence, M.G., Lelieveld, J., 2010. Atmospheric pollutant outflow from Southern Asia: a review. Atmos. Chem. Phys. 10:11017–11096. http://dx.doi.org/10.5194/acp-10-11017-2010.

Lelieveld, J., Crutzen, P.J., Ramanathan, V., Andreae, M.O., Brenninkmeijer, C.A.M., Campos, T., Cass, G.R., Dickerson, R.R., Fischer, H., de Gouw, J.A., Hansel, A., Jefferson, A., Kley, D., de Laat, A.T.J., Lal, S., Lawrence, M.G., Lobert, J.M., Mayol-Bracero, O.L., Mitra, A.P., Novakov, T., Oltmans, S.J., Prather, K.A., Reiner, T., Rodhe, H., Scheeren, H.A., Sikka, D., Williams, J., 2001. The Indian Ocean Experiment: widespread air pollution from south and Southeast Asia. Science 1031–1036.

Lewis, K.A., Arnott, W.P., Moosmuller, H., Chakrabarty, R.K., Carrico, C.M., Kreidenweis, S.M., Day, D.E., Malm, W.C., Laskin, A., Jimenez, J.L., Ulbrich, I.M., Huffman, J.A., Onasch, T.B., Trimborn, A., Liu, L., Mishchenko, M.I., 2009. Reduction in biomass burning aerosol light absorption upon humidification: roles of inorganically-induced hygroscopicity, particle collapse, and photoacoustic heat and mass transfer. Atmos. Chem. Phys. 9:8949–8966. http://dx.doi.org/10.5194/acp-9-8949-2009.

Li-Jones, X., Maring, H.B., Propero, J.M., 1998. Effect of relative humidity on light scattering by mineral dust aerosol as measured in the marine boundary layer over the tropical Atlantic Ocean. J. Geophys. Res. 103, 31113–31121.

Liu, X., Zhang, Y., Jung, J., Gu, J., Li, Y., Guo, S., Chang, S.-Y., Yue, D., Lin, P., Kim, Y.J., Hu, M., Zeng, L., Zhu, T., 2009. Research on the hygroscopic properties of aerosols by measurement and modeling during CAREBeijing-2006. J. Geophys. Res. 114, D00G16. http://dx.doi.org/10.1029/2008JD010805.

Lohmann, U., Feichter, J., 2005. Global indirect aerosol effects: a review. Atmos. Chem. Phys. 5, 715–737.

Lu, Z., Zhang, Q., Streets, D.G., 2011. Sulfur dioxide and primary carbonaceous aerosol emissions in China and India, 1996–2010. Atmos. Chem. Phys. 11:9839–9864. http://dx.doi.org/10.5194/acp-11-9839-2011.

Magi, B.I., Hobbs, P.V., 2003. Effects of humidity on aerosols in Southern Africa during the biomass burning season. J. Geophys. Res. 108 (D13), 8495.

Malm, W.C., Kreidenweis, S.M., 1997. The effects of models of aerosol hygroscopicity on the apportionment of extinction. Atmos. Environ. 31 (13), 1965–1976.

Malm, W.C., Day, D.E., Kreidenweis, S.M., Collett Jr., J.L., Carrico, C.M., McMeeking, G., Lee, T., 2005. Hygroscopic properties of an organic-laden aerosol. Atmos. Environ. 39, 4969–4982.

Manoharan, V.S., Kotamarthi, R., Feng, Y., Cadeddu, M.P., 2014. Increased absorption by coarse aerosol particles over the Gangetic-Himalayan region. Atmos. Chem. Phys. 14:1159–1165. http://dx.doi.org/10.5194/acp-14-1159-2014.

McInnes, L., Bergin, M., Ogren, J.A., Schwartz, S., 1998. Apportionment of light scattering and hygroscopic growth to aerosol composition. Geophys. Res. Lett. 25 (4), 513–516.

Mircea, M., Facchini, M.C., Decesari, S., Cavalli, F., Emblico, L., et al., 2005. Importance of the organic aerosol fraction for modelling aerosol hygroscopic growth and activation: a case study in the Amazon Basin. Atmos. Chem. Phys. 5, 3111–3126.

Moorthy, K.K., Satheesh, S.K., Kotamarthi, V.R., 2016. Evolution of aerosol research in India and the RAWEX–GVAX: an overview. Curr. Sci. 111, 53–75.

Nessler, R., Weingartner, E., Baltensperger, U., 2005. Adaptation of dry Nephelometer measurements to ambient conditions at the Jungfraujoch. Environ. Sci. Technol. 39, 2219–2228.

Pagels, J., Khalizov, A.F., McMurry, P.H., Zhang, R.Y., 2009. Processing of soot by controlled sulphuric acid and water condensation—mass and mobility relationship. Aerosol Sci. Technol. 43, 629–640.

Pan, X.L., Yan, P., Tang, J., Ma, J.Z., Wang, Z.F., Gbaguidi, A., Sun, Y.L., 2009. Observational study of influence of aerosol hygroscopic growth on scattering coefficient over rural area near Beijing mega-city. Atmos. Chem. Phys. 9:7519–7530. http://dx.doi.org/10.5194/acp-9-7519-2009.

Perry, K.D., Cliff, S.S., Jimenez-Cruz, M.P., 2004. Evidence for hygroscopic mineral dust particles from the Intercontinental Transport and Chemical Transformation Experiment. J. Geophys. Res. 109, D23S28. http://dx.doi.org/10.1029/2004JD004979.

Quinn, P.K., Bates, T.S., Baynard, T., Clarke, A.D., Onasch, T.B., Wang, W., et al., 2005. Impact of particulate organic matter on the relative humidity dependence of light scattering: a simplified parameterization. Geophys. Res. Lett. 32, L22809.

Rajput, P., Sarin, M., Sharma, D., Singh, D., 2014. Characteristics and emission budget of carbonaceous species from post-harvest agricultural-waste burning in source region of the Indo-Gangetic Plain. Tellus B66:21026. http://dx.doi.org/10.3402/tellusb.v66.21026.

Ram, K., Sarin, M.M., Hegde, P., 2010a. Long-term record of aerosol optical properties and chemical composition from a high-altitude site (Manora Peak) in Central Himalaya. Atmos. Chem. Phys. 10:11791–11803. http://dx.doi.org/10.5194/acp-10-11791-2010.

Ram, K., Sarin, M.M., Tripathi, S.N., 2010b. A 1-year record of carbonaceous aerosols from an urban site in the Indo-Gangetic Plain: characterization, sources, and temporal variability. J. Geophys. Res. 115, D24313. http://dx.doi.org/10.1029/2010JD014188.

Rastogi, N., Singh, A., Singh, D., Sarin, M.M., 2014. Chemical characteristics of $PM_{2.5}$ at a source region of biomass burning emissions: evidence for secondary aerosol formation. Environ. Pollut. 184, 563–569.

Reid, J.S., Eck, T.F., Christopher, S.A., Koppmann, R., Dubovik, O., Eleuterio, D.P., Holben, B.N., Reid, E.A., Zhang, J., 2005. A review of biomass burning emissions part III: intensive optical properties of biomass burning particles. Atmos. Chem. Phys. 5, 827–849.

Robert, G.C., Nenes, A., 2005. A continuous flow streamwise thermal gradient CCN chamber for atmospheric measurements. Aerosol Sci. Technol. 39, 206–221.

Rosenfeld, D., Lohmann, U., Raga, G.B., et al., 2008. Flood or drought: how do aerosols affect precipitation? Science 321 (5894), 1309–1313.

Sheridan, P.J., Delene, D.J., Ogren, J.A., 2001. Four years of continuous surface aerosol measurements from the Department of Energy's atmospheric radiation measurement program southern Great Plains cloud and radiation testbed site. J. Geophys. Res. 106, 20735–20747.

Sheridan, P.J., Jefferson, A., Ogren, J.A., 2002. Spatial variability of submicrometer aerosol radiative properties over the Indian Ocean during INDOEX. J. Geophys. Res. 107: 8011. http://dx.doi.org/10.1029/2000JD000166.

Shi, Z., Zhang, D., Hayashi, M., et al., 2007. Influences of sulfate and nitrate on the hygroscopic behaviour of coarse dust particles. Atmos. Environ. 42 (4), 822–827.

Shingler, T., Sorooshian, A., Ortega, A., Crosbie, E., Wonaschütz, A., Perring, A.E., Beyersdorf, A., Ziemba, L., Jimenez, J.L., Campuzano-Jost, P., Mikoviny, T., Wisthaler, A., Russell, L.M., 2016a. Ambient observations of hygroscopic growth factor and f(RH) below 1: case studies from surface and airborne measurements. J. Geophys. Res. 121, 13,661–13,677.

Shingler, T., Crosbie, E., Ortega, A., Shiraiwa, M., Zuend, A., Beyersdorf, A., Ziemba, L., Anderson, B., Thornhill, L., Perring, A.E., Schwarz, J.P., Campazano-Jost, P., Day, D.A., Jimenez, J.L., Hair, J.W., Mikoviny, T., Wisthaler, A., Sorooshian, A., 2016b. Airborne characterization of subsaturated aerosol hygroscopicity and dry refractive index from the surface to 6.5 km during the SEAC4RS campaign. J. Geophys. Res. 121, 4188–4210.

Shinozuka, Y., Johnson, R.R., Flynn, C.J., Russell, P.B., Schmid, B., Redemann, J., Dunagan, S.E., Kluzek, C.D., Hubbe, J.M., Segal-Rosenheimer, M., Livingston, J.M., Eck, T.F., Wagener, R., Gregory, L., Chand, D., Berg, L.K., Rogers, R.R., Ferrare, R.A., Hair, J.W., Hostetler, C.A., Burton, S.P., 2013. Hyperspectral aerosol optical depths from TCAP flights. J. Geophys. Res. Atmos. 118:12180–12194. http://dx.doi.org/10.1002/2013JD020596.

Tijjani, B.I., Uba, S., 2013. The Effect of Hygroscopic Growth on Urban Aerosols. 25. The International Institute for Science, Technology and Education (IISTE), pp. 58–75.

Tijjani, B.I., Aliyu, A., Shaaibu, F., 2014. The effect of relative humidity on continental average aerosols. Open J. Appl. Sci. 4, 399–423.

Titos, G., Jefferson, A., Sheridan, P.J., Andrews, E., Lyamani, H., Alados-Arboledas, L., Ogren, J.A., 2014a. Aerosol light-scattering enhancement due to water uptake during the TCAP campaign. Atmos. Chem. Phys. 14:7031–7043. http://dx.doi.org/10.5194/acp-14-7031-2014.

Titos, G., Lyamani, H., Cazorla, A., Sorribas, M., Foyo-Moreno, I., Wiedensohler, A., Alados-Arboledas, L., 2014b. Study of the relative humidity dependence of aerosol light-scattering in southern Spain. Tellus Ser. B Chem. Phys. Meteorol. 2014 (66):24536. http://dx.doi.org/10.3402/tellusb.v66.24536.

Titos, G., Cazorla, A., Zieger, P., Andrews, E., Lyamani, H., Granados-Munoz, M.J., Olmo, F.J., Alados-Arboledas, L., 2016. Effect of hygroscopic growth on the aerosol light-scattering coefficient: a review of measurements, techniques and error sources. Atmos. Environ. 141, 494–507.

Wang, J., Martin, S.T., 2007. Satellite characterization of urban aerosols: importance of including hygroscopicity and mixing state in the retrieval algorithms. J. Geophys. Res. 112, D17203. http://dx.doi.org/10.1029/2006JD008078.

Wang, W., Rood, M.J., Carrico, C.M., Covert, D.S., Quinn, P.K., Bates, T.S., 2007. Aerosol optical properties along the northeast coast of North America during the New England Air Quality Study–Intercontinental Transport and Chemical Transformation 2004 campaign and the influence of aerosol composition. J. Geophys. Res. 112, D10S23. http://dx.doi.org/10.1029/2006JD007579.

WMO/GAW, 2003. Aerosol Measurement Procedures Guidelines and Recommendations, GAWRep. 153. World Meteorol Organ, Geneva, Switzerland available at. ftp://ftp.wmo.int/Documents/PublicWeb/arep/gaw/gaw153.pdf (last access: July 2014).

Yan, P., Pan, X., Tang, J., Zhou, X., Zhang, R., Zeng, L., 2009. Hygroscopic growth of aerosol scattering coefficient: a comparative analysis between urban and suburban sites at winter in Beijing. Particuology 7, 52–60.

Youn, J.-S., et al., 2016. Hygroscopic properties and respiratory system deposition behavior of particulate matter emitted by mining and smelting operations. Environ. Sci. Technol. 50:11706–11713. http://dx.doi.org/10.1021/acs.est.6b03621.

Zhang, L., Sun, J.Y., Shen, X.J., Zhang, Y.M., Che, H.C., Ma, Q.L., Zhang, Y.W., Zhang, X.Y., Ogren, J.A., 2015. Observations of relative humidity effects on aerosol light scattering in the Yangtze River Delta of China. Atmos. Chem. Phys. 15, 8439–8454.

Zieger, P., Fierz-Schmidhauser, R., Gysel, M., Ström, J., Henne, S., Yttri, K.E., Urs, Baltensperger, Weingartner, E., 2010. Effects of relative humidity on aerosol light scattering in the Arctic. Atmos. Chem. Phys. 10:3875–3890. http://dx.doi.org/10.5194/acp-10-3875-2010.

Zieger, P., Weingartner, E., Henzing, J., Moerman, M., de Leeuw, G., Mikkilä, J., Ehn, M., Petäjä, T., Clémer, K., van Roozendael, M., Yilmaz, S., Frieß, U., Irie, H., Wagner, T., Shaiganfar, R., Beirle, S., Apituley, A., Wilson, K., Baltensperger, U., 2011. Comparison of ambient aerosol extinction coefficients obtained from in-situ, MAX-DOAS and LIDAR measurements at Cabauw. Atmos. Chem. Phys. 11:2603–2624. http://dx.doi.org/10.5194/acp-11-2603-2011.

Zieger, P., Kienast-Sjögren, E., Starace, M., von Bismarck, J., Bukowiecki, N., Baltensperger, U., Wienhold, F.G., Peter, T., Ruhtz, T., Collaud Coen, M., Vuilleumier, L., Maier, O., Emili, E., Popp, C., Weingartner, E., et al., 2012. Atmos. Chem. Phys. 12:7231–7249. http://dx.doi.org/10.5194/acp-12-7231-2012.

Zieger, P., Fierz-Schmidhauser, R., Weingartner, E., Baltensperger, U., 2013. Effects of relative humidity on aerosol light scattering: results from different European sites. Atmos. Chem. Phys. 13:10609–10631. http://dx.doi.org/10.5194/acp-13-10609-2013.

Zieger, P., Fierz-Schmidhauser, R., Poulain, L., Müller, T., Birmili, W., Gerald, Spindler, Alfred, Wiedensohler, Urs, Baltensperger, Ernest, Weingartner, 2014. Influence of water uptake on the aerosol particle light scattering coefficients of the Central European aerosol. Tellus Ser. B Chem. Phys. Meteorol. 66:22716. http://dx.doi.org/10.3402/tellusb.v66.22716.